TECHNISCHE UNIVERSITÄT WIEN
Vienna University of Technology

D I P L O M A R B E I T

Influence of the spinal curvature on the efficacy of transcutaneous stimulation of the human lumbar spinal cord

Ausgeführt am

Institut für Analysis und Scientific Computing

der Technischen Universität Wien

unter der Anleitung von

Ao.Univ.Prof. Dipl.-Ing. DDDr. Frank Rattay,

Mag. Dipl.-Ing. Dr.techn. Simon Danner

und

Dipl.-Ing. Dr.med.univ. Anna Rienmüller

durch

Veronika Binder

Anastasius Grüngasse 41a

1180, Wien

Wien, 18.11.2015

Veronika Binder

Acknowledgements

First and foremost, I want to thank Professor Frank Rattay for his expert supervision and scientific support, which is greatly appreciated.

This thesis would not have been possible without the guidance of Dr. Simon Danner, who, with his expertise and commitment, supported me with this study right from the development of the measurement protocol and data analysis, up to the completion of this thesis, whether while on site or overseas.

Furthermore, I want to thank Dr. Matthias Krenn for his technical advisement and help with the measurements, as well as Dr. Anna Rienmueller for her medical input, Dr. Karen Minassian for his crucial help in developing the measurement protocol and Dr. Ursula Hofstoetter for her expertise.

Thanks to my colleagues for lending a hand during my measurements and to the volunteers who readily endured the lengthy and not always comfortable stimulation.

Finally, I am grateful to my wonderful parents, who have supported and encouraged me throughout my studies.

Abstract

Elicitation of spinal reflexes and effective neuromodulation by transcutaneous spinal cord stimulation (tSCS) relies on selective activation of sensory fibers within the spinal roots. Activation thresholds of sensory and motor nerves at spinal cord level depend on the geometry and electric properties of the surrounding tissue. The well conducting intervertebral discs allow current to enter the spinal canal where the roots are located and the flexion and extension of the spine alters their shape and position. Hence we hypothesize that the spinal curvature influences the activation thresholds of sensory and motor fibers within the roots.

We evoked bilateral responses to tSCS administered between T11 and T12 vertebrae in quadriceps, hamstrings, tibialis anterior and soleus in ten neurologically intact subjects, and compared both maximal dorsi- and ventralflexion to a neutral spine in four different body positions, supine, lateral, sitting and standing. Single and paired (35 ms inter-stimulation interval) biphasic pulses were used to study response amplitudes and differentiate between preferential sensory posterior or motoric anterior root fiber stimulation. To control for posturally induced reflex pathway gain alterations, we simultaneously evoked soleus H reflexes in each subject and kept the H reflex amplitudes constant between spinal curvatures, to ensure spinal reflex amplitudes reflected tSCS effectiveness rather than reflex pathway gain.

Ventralflexion significantly decreased tSCS efficacy, lowering muscle response amplitudes to single stimuli across all positions and increasingly favoring direct motoneuron activation during sitting and standing. Dorsiflexion, on the other hand, showed no change in responses. Our results suggest an unfavorable transversal current density distribution within and around the spinal canal as a result of ventralflexion of the spine. We therefore recommend tSCS stimulation with a straight or dorsiflexed spine to reliably and effectively evoke spinal reflexes.

Zusammenfassung

Das Auslösen von Spinalreflexen und effektive Neuromodulation durch transkutane Rückenmarkstimulation bedarf selektiver Aktivierung der sensorischen Nervenfasern der Spinalwurzeln. Die Aktivierungsschwellen der sensorischen und motorischen Nervenwurzeln hängen von der Geometrie und den elektrischen Eigenschaften des umgebenden Gewebes ab. Strom tritt größtenteils durch die gut leitenden Bandscheiben in den Wirbelkanal ein, in dem sich die Spinalwurzeln befinden. Vorwärts- oder Rückwärtskrümmung verändert Form und Position der Bandscheiben. Daher stellten wir die Hypothese auf, dass die Krümmung der Wirbelsäule die Aktivierungsschwellen der sensorischen und motorischen Nervenfasern beeinflusst.

Wir lösten mit transkutaner Rückenmarkstimulation, appliziert zwischen den T11 und T12 Wirbeln, bilaterale Antworten in Quadriceps, Hamstrings, Tibialis Anterior und Soleus bei zehn neurologisch intakten Probanden aus, und verglichen sowohl Rückwärts- als auch Vorwärtskrümmung mit neutraler Wirbelsäulenhaltung in vier verschiedenen Körperpositionen, Rückenlage, Seitenlage, Sitzen und Stehen. Wir verwendeten biphasische Einzel- und Doppelpulse (35 ms Interstimulusintervall), um sowohl Antwortamplituden als auch deren Ursprung – eine Zusammensetzung aus sensorischer Hinterwurzel- und motorischer Vorderwurzelstimulation – zu analysieren. Um Beeinflussung der Ergebnisse durch Reflexbogenmodifikation zu vermeiden, lösten wir bei jedem Probanden zusätzlich H Reflexe in einem Soleus aus und hielten deren Amplituden konstant.

Vorwärtskrümmung verminderte die Effektivität der transkutanen Rückenmarkstimulation stark: Muskelantworten wurden kleiner und direkte Motorstimulation fand, vor allem im Sitzen und Stehen, statt. Rückwärtskrümmung hingegen zeigte keinerlei Veränderungen. Unsere Ergebnisse weisen auf eine durch Vorwärtskrümmung bewirkte, nachteilhafte transversale Stromdichteverteilung innerhalb und um den Wirbelkanal hin. Daher empfehlen wir transkutane Rückenmarkstimulation mit geradem Rücken (oder Rückwärtskrümmung) durchzuführen, um verlässlich und effektiv Spinalreflexe auszulösen.

Abbreviations

A_1	peak to peak amplitude of single pulse responses from tSCS
A_2	peak to peak amplitude of second stimulation pulse responses from tSCS with double pulses
A_H	peak to peak amplitude of main soleus from peripheral H reflex stimulation
A_M	peak to peak amplitude of M wave elicited during H reflex stimulation
A_{tSCS}	peak to peak amplitude of main soleus from tSCS
AP	action potential
CMAP	compound muscle action potential
EPSP	excitatory postsynaptic potential
H	hamstrings
H reflex	Hoffmann reflex
I_H	stimulation intensity of H reflex stimulation
I_{tSCS}	stimulation intensity of tSCS
IPSP	inhibitory postsynaptic potential
ISI	inter-stimulus interval
M_{max}	maximal obtainable amplitude of M wave
M wave	CMAP evoked by direct motoneuron stimulation
PRM reflex	posterior root-muscle reflex
PS	peripheral stimulation
Q	quadriceps
S	soleus
SCS	spinal cord stimulation
TA	tibialis anterior
TS	triceps surae
tSCS	transcutaneous spinal cord stimulation

Contents

Acknowledgements i

Abstract iii

Zusammenfassung iv

Abbreviations v

1. Introduction 1

2. Anatomic and physiological background 4

2.1. The nerve cell 4

2.2. Anatomy of the human spinal cord 6

2.3. Spinal reflex pathways 9

2.4. Transcutaneous electrical stimulation of the lumbar spinal cord 11

2.5. The Hoffmann reflex 16

2.6. Comparison of PRM and H reflex 18

3. Methods 20

3.1. Subjects 20

3.2. Stimulation and Recording Setup 21

3.3. Positions 23

3.4. Measuring Protocol 24

3.5. Data Acquisition and Processing 25

3.6. Statistic Analysis 27

4. Results 29

4.1. Main soleus 29

First response amplitudes 29

Ratio of second to the first response amplitude 31

4.2. All Muscles 33

First response amplitude 34

Ratio of second to first response amplitude 37
5. Discussion 40
5.1. Relative excitation thresholds of stimulation hotspots 40
5.2. H reflex controlled main soleus: exclusion of reflex gain influences 42
5.3. All muscle groups 44
6. Conclusion 47
Bibliography 48

1. Introduction

Electrical spinal cord stimulation (SCS) has proven to be a promising tool for restoration and improvement of lower limb function after spinal cord injuries. Even without the connection to supraspinal inputs, the intrinsic function of the spinal cord caudal to the injury remains. The lumbar spinal cord has been demonstrated to have neuronal networks that control motor function of the lower limbs, which can be activated by SCS with implanted, epidural electrodes (Dimitrijevic, et al., 1998). Depending on the stimulation frequency, SCS with implanted, epidural electrodes can produce a variety of movements, from simple limb extension (Jilge, et al., 2004; Minassian, et al., 2007a) to patterned, step-like movements in a supine position without the proprioceptive feedback that can be provided by passive treadmill stepping (Shapkova, 2004; Minassian, et al., 2005; Minassian, et al., 2007a; Danner, et al., 2015). Weight-baring standing without manual facilitation (Harkema, et al., 2011) and even partial restoration of voluntary motor control (Angeli, et al., 2014) has been observed. Additionally, epidural SCS has been shown useful in the control of spinal spasticity in individuals with spinal cord injury and multiple sclerosis (Cook & Weinstein, 1973; Cook, 1976; Dimitrijevic, et al., 1986; Pinter, et al., 2000).

Transcutaneous stimulation (tSCS) using commercially available self-adhesive surface electrodes has all the advantages of a non-invasive method, while still providing similar efficacy in alleviation of spinal spasticity (Hofstoetter, et al., 2014a), as well as improved gait (Minassian, et al., 2012a; Hofstoetter, et al., 2014b; Minassian, et al., 2015). Despite the, in comparison to epidural stimulation, diffuse electrical field, the same type of neural structures, the posterior roots containing peripheral afferent fibers, are excited. Single stimulation pulses elicit posterior root-muscle reflexes, i.e., arguably monosynaptic reflexes similar to the H reflex in all lower limb muscles simultaneously (Minassian et al., 2007).

Recently, tSCS has been performed by several groups (Courtine, et al., 2007; Kitano & Koceja, 2009; Roy, et al., 2012; Knikou, 2013) using different body positions, such as supine, prone, sitting and standing, with varying results. Some studies reported selective sensory nerve while others also found concomitant motor nerve activation. Yet, for neuromodulation applications it is essential that sensory fibers are selectively stimulated (Holsheimer, 1998a) and these discrepancies can only be partially explained by the finding that the supine and standing positions favor sensory and the prone position motor nerve stimulation (Danner et al., submitted).

Computational studies have found three low threshold sites: i) at the entry of the posterior root (sensory) fibers into the spinal cord, ii) at the exit of the anterior root (motor) fibers from the spinal cord, and iii) at their common transition from the spinal canal through the vertebral foramina (Rattay, et al., 2000; Ladenbauer, et al., 2010; Danner, et al., 2011; Danner, et al., 2014). The relative excitability of these hotspots is a result of non-uniformities of the geometry of the neuronal fibers as well as the surrounding tissue conductivities and depends on the local current density and directionality of the electric field. Since the current density distribution within the spinal column depends on the relative geometry of the spinous processes and the more conductive (factor 30 (Szava, 2006)) intervertebral disks and ligaments, we hypothesize that the spinal curvature at the level of stimulation, especially in the sagittal plane, influences the efficacy of tSCS, whether by diminishing posterior root (by increasing the threshold of hotspot i) or favoring anterior root excitation (by decreasing threshold of hotspot ii and iii). Further understanding the biophysical mechanisms of tSCS will give insight into which postures or positions can impede reflex elicitation, and how to reliably evoke spinal reflexes. Especially during (weight-supported) walking, but also for slouched sitting or supine positions with a propped up upper body, forward or backward curvature of the lumbar spine could be a limiting factor in the stimulation effectuality. In this work, we investigate whether

and how sagittal spinal curvature influences tSCS efficacy in neurologically intact individuals.

2. Anatomic and physiological background

This chapter will give a short overview of the human spinal nervous system, before covering relevant reflex mechanisms of the lower extremities as well as biophysical aspects of tSCS.

2.1. The nerve cell

Neurons are electrically active cells that, along with glia cells, make up the nervous system, transmitting information by producing electric signals called action potentials (AP) in response to mechanical, chemical or electrical stimuli. They consist of the nucleus within the soma, dendrites and an axon (Figure 1), though some types of neurons lack axons or dendrites.

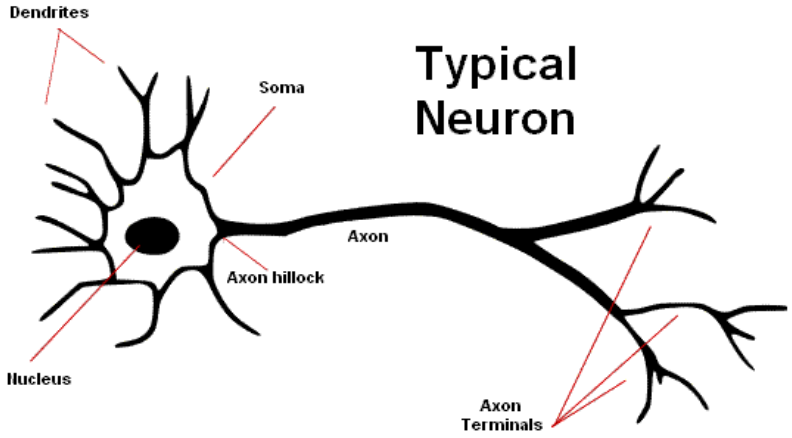

Figure 1 – Structure of a myelinated neuron. Temporal and spatial summation of membrane depolarization of the dendrites leads to the generation of an AP at the axon hillock, which travels along the axon to the terminals and synapses to the subsequent neurons (Beam-Wiki, 2014).

The neuron's membrane is an insulating lipid bilayer with embedded ion channels and pumps that transport ion across the membrane, generating concentration and electric gradients. When the neuron is inactive, its resting membrane potential is approximately -70 mV (difference between intracellular to extracellular potential). By

opening receptive ion channels located in the dendrite membrane, signals are received along the multiple thin branches of the dendrites and produce a change in electric membrane potential that spreads along the dendrite and soma membrane, decreasing exponentially (passive conduction). If this potential change reaches the axon hillock and is above a certain threshold, about -50 mV (Kandel, et al., 2013), an AP will be generated and propagate along the axon. Therefore, the generation of an AP and subsequent signal transmission of the neuron is facilitated by spatial and temporal summation of multiple signals in the dendrites.

As described in Kandel, et al., 2013, the AP of a neuron, once generated, always exhibits the same temporal behavior, regardless of the triggering membrane potential, as long as it is above this threshold. This is caused by a characteristic reaction by active ion channels of the axon to sufficiently high depolarization: fast opening, voltage-gated Na^+ channels are activated and allow Na^+ ions to flow into the cell, depolarizing it further. The slower K^+ channels react upon this potential change by allowing K^+ ions to flow out of the cell, repolarizing the membrane. Meanwhile, the Na^+ channels deactivate rapidly and need a certain time before they can be activated again, resulting in an absolute refractory period following the generation of an AP, when none of the Na^+ channels can be activated again, and a subsequent relative refractory period where only some of the Na^+ channels are able to open again and an AP can only be elicited by a stronger stimulus. The duration of both refractory periods combined is about 5-10 ms. This helps code the strength of the stimulus received by the neuron, since the AP's amplitude remains constant: stronger stimuli can elicit the next AP sooner during the relative refractory period, resulting in a higher AP frequency.

The AP travels along the axon, depolarizing neighboring Na^+ channels and thereby eliciting new APs. Because of the refractory period, the AP propagates only in one direction along the axon under natural conditions. Myelinated neurons have isolating

glia cells, called Schwann's cells, surrounding their axons to allow fast signal transmission of up to 120 m/s; the equalizing currents induced by an AP activate the next uninsulated ion channels at the nodes of Ranvier. At the axon terminal, the neuron is usually connected to neighboring neuron dendrites through a chemical synapse. When the AP reaches the presynaptic terminal at the end of the axon, it causes an inflow of Ca^{2+} ions, which in turn induces the release of a certain quantity of neurotransmitters into the synaptic cleft, which bind to the chemically gated ion channels of the postsynaptic membrane of the next neuron. Depending on the neurotransmitter and its corresponding ion channels, a presynaptic potential can either elicit an excitatory postsynaptic potential (EPSP) or an inhibitory postsynaptic potential (IPSP). These chemical synapses take more time in comparison to electric AP transmission, up to several milliseconds depending on the type of chemical synapse (Kandel, et al., 2013). It should also be noted that, while axons usually connect to dendrites of the next axon, axon-soma, axon-axon or dendrite-dendrite connections can also occur. These mechanisms allow neurons to form large, functionally diverse networks.

2.2. Anatomy of the human spinal cord

As part of the central nervous system, the human spinal cord contains long afferent and efferent neurons responsible for transmitting information between the brain and peripheral nervous system, as well as neuronal networks which control reflexes. It is surrounded by three meningens, similar to the brain, with the outermost dura mater only attached to the foramen magnum and the uppermost cervical vertebra. For the remaining length of the spinal column, the spinal cord is untethered to the vertebrae and separated from them by the epidural space (O'Rahilly, et al., 2004). At the segmental levels depicted in Figure 2, the 31 pairs of peripheral spinal nerves originate from the spinal cord and project to muscles and sensory endings. The spinal cord is shorter than the encasing spinal column, reaching from the foramen magnum

of the skull to the T12-L3 level of the spine (O'Rahilly, et al., 2004), where the lower spinal nerves continue to run parallel within the spinal canal, forming the cauda equina, until they exit the spinal column at their eponymous vertebra. Because of this length disparity, the more caudal spinal roots are bent downward at their exit point from the spinal cord, whereas cervical roots run perpendicular to the spinal cord and exit the spinal column almost at the same level as they originate from the spinal cord.

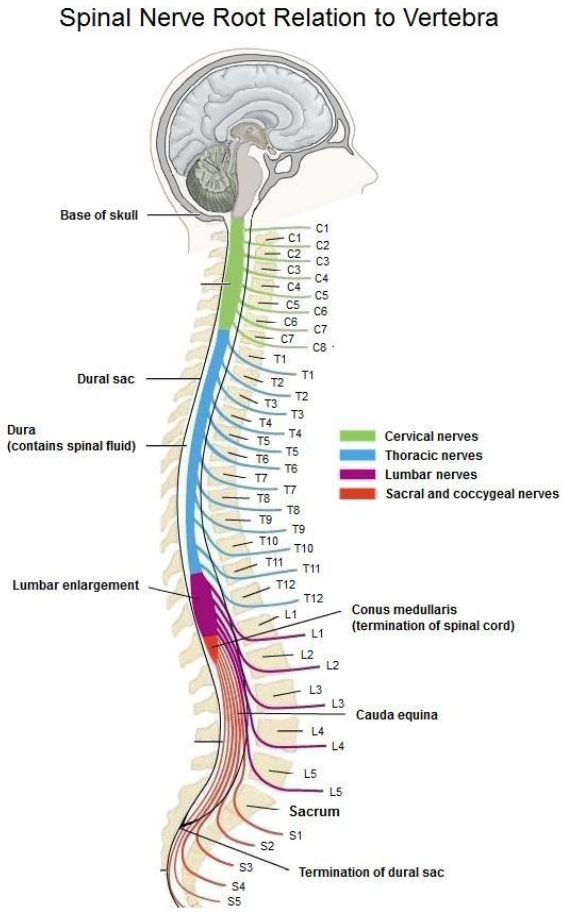

Figure 2 – The relation between spinal nerves and vertebral levels; at caudal levels, the spinal nerves run parallel to the spinal cord within the spinal column. (My-MS, 2014)

The afferent fibers transition into dorsal horn of the gray matter of the spinal cord at the posterior (or dorsal) root, while the α-motoneurons, whose axons exit the spinal cord at the anterior (or ventral) root, are located in the ventral horn. These areas are surrounded by white matter containing the ascending and descending tracts of the spinal cord, while the gray matter is mainly composed of cell bodies (Figure 3).

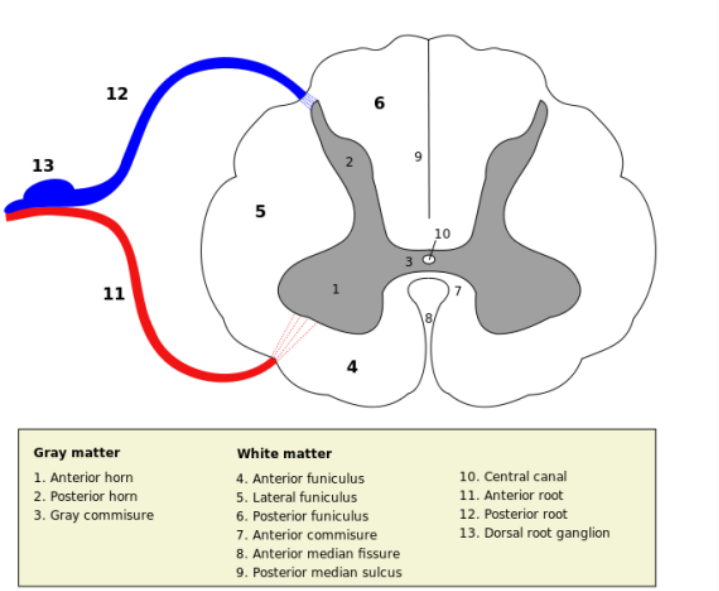

Figure 3 – Horizontal Spinal Cord Section; afferent volleys enter the gray matter through the posterior root and horn, efferent volleys through the anterior horn and root. (Wikipedia, 2014)

The main afferents involved in locomotive reflexes are type Ia, Ib and II fibers, which sense muscle movement, tension and length. Ia and II fibers innervate the muscle spindles, proprioceptors located within the muscles, parallel to the contractile muscle fibers. Ia fibers are myelinated and the thickest of the three afferent fibers (Pierrot-Deseilligny & Burke, 2012), providing the fastest conduction of information about muscle length and the velocity of stretching (Kandel, et al., 2013). Type II fibers are slightly thinner and predominantly sense static muscle length. Both afferents are activated by mechanically gated ion channels (Purves, et al., 2004) and the resulting

afferent volleys are relayed to α-motoneurons that evoke a contraction in the homonymous muscle. Ib fibers relay information about muscle tension from passive stretching as well as active contraction (Purves, et al., 2004). Their endings are wrapped around collagen fibrils within the Golgi tendon organ, located at the transition of muscle into tendon. Generally, Ia afferents have the lowest stimulation thresholds and fastest signal conduction (Pierrot-Deseilligny & Burke, 2012).

2.3. Spinal reflex pathways

The above described projection is referred to as a monosynaptic reflex, directly connecting afferent fibers and motoneurons. To coordinate more complex movements, polysynaptic pathways with excitatory or inhibitory interneurons as well as reflex loops involving corticospinal and vestibular inputs are used to alter the reflex gain (Pierrot-Deseilligny & Burke, 2012).

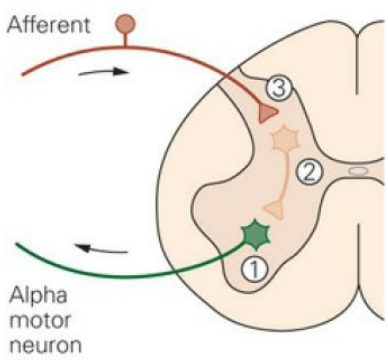

Figure 4 – Sites of reflex modification within the spinal cord: at α-motoneuron (1), interneurons (2) and afferent axon terminals (3). (Kandel, et al., 2013)

Every reflex pathway can be modified at three sites within the spinal cord (Kandel, et al., 2013): the α-motoneuron, interneurons, or the afferent axon terminal (Figure 4). A large number of reflex modification pathways have been investigated. The basic mechanisms that can result in reflex gain changes for different static positions will be described here.

The stretch reflex (Figure 5), for instance, gives a good overview of the interconnections between different muscles by Ia afferents: when the muscle is stretched and therefore its Ia fiber firing rate increased, this afferent not only projects monosynaptically to the homonymous muscle, but also to the synergistic and, over inhibitory interneurons, to antagonistic motoneurons, effectively counteracting the stretch. Conversely, the opposite effect has been observed in the contralateral limb: muscles that are stretched in one limb are inhibited on the contralateral side, and vice versa. Generally, the EPSP evoked by a Ia afferent is larger in the homonymous muscle than heteronymous muscles, where only a few motoneurons out of the available motoneuron pool are accessed by this Ia fiber's terminals (Pierrot-Deseilligny & Burke, 2012). Ib and II fibers have been found to have projections to antagonists and synergists as well (Pierrot-Deseilligny & Burke, 2012). Therefore, length and position – as well as electric stimulation of afferent fibers - of one muscle can modify the reflex pathways of several others.

Proprioreceptive feedback is not only processed at the spinal level, though. Long latency transcortical Ia reflex pathways projecting to the homonymous α-motoneuron have been observed, for the lower limbs mainly in the tibialis anterior, as well as medium latency transcortical pathways involving type II afferents (Pierrot-Deseilligny & Burke, 2012). Additionally, studies using transcranial magnetic stimulation (Kudina, et al., 1993; Nielsen, et al., 1993; Meunier & Pierrot-Deseilligny, 1998) have demonstrated an influence of descending corticospinal inputs on reflex facilitation, pathways that project directly to motoneurons as well as to the Ia presynaptic terminals via interneurons (Pierrot-Deseilligny & Burke, 2012). Vestibular inputs have also been shown to modify reflex gain through Ia presynaptic inhibition and alteration of reciprocal Ia inhibition (Iles & Pisini, 1992; Rossi, et al., 1988).

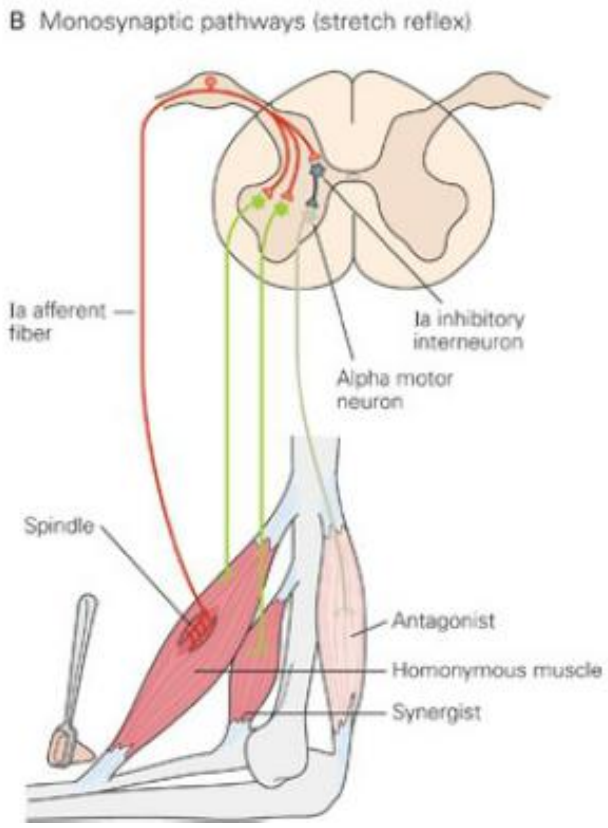

Figure 5 – Sketch of stretch reflex pathways: Ia fibers project to the motoneurons of the homonymous muscle as well as antagonists and synergists. (Kandel, et al., 2013)

2.4. Transcutaneous electrical stimulation of the lumbar spinal cord

Lumbar spinal cord stimulation can produce rhythmic, locomotion-like movement of reflex nature in the lower limbs, even in the absence of supraspinal input. These reflexes have been named posterior root-muscle reflexes (PRM reflexes) according to their initiation and recording site, the muscles of the lower limbs (Jilge, et al., 2004; Minassian, et al., 2004; Minassian, et al., 2007a). Different pathways and mechanisms for this reflex have been identified; while low repetition rates, about 1 Hz, produce PRM reflexes with monosynaptic pathways that result in extension-like lower limb movement, where the elicited compound muscle action potentials have constant latencies, waveforms and peak to peak amplitudes (Figure 6) (Minassian, et al.,

2012a), higher stimulation frequencies (25-50 Hz) result in activation of lumbar locomotor circuits – specific neuronal networks – in the spinal cord, which cause rhythmic, step-like flexion and extension of the lower limb, even in the absence of supraspinal input (Dimitrijevic, et al., 1998; Minassian, et al., 2004; Minassian, et al., 2007a; Minassian, et al., 2012a). The data from electrophysiological (Murg, et al., 2000; Minassian, et al., 2004) and computational (Rattay, et al., 2000; Ladenbauer, et al., 2010) studies suggest a two-fold effect of tonic drive to the lumbar spinal cord via the afferent posterior roots: transsynaptic muscle responses at the corresponding spinal segments as well as transsynaptic co-activation of lumbar interneuronal circuits (Minassian, et al., 2012b). The reflex origin of the elicited muscle twitches is corroborated by the depression of excitability after previous stimulation for up to ten seconds (post-activation depression) (Minassian, et al., 2009), as well as during tendon vibration and active or passive movement (Minassian, et al., 2007b).

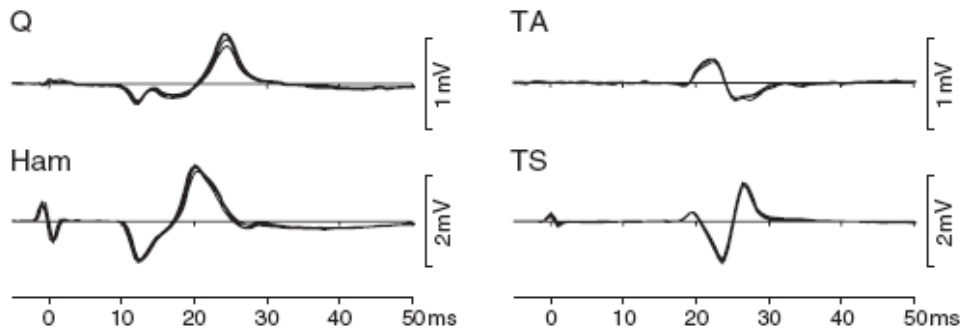

Figure 6 – EMG recording of PRM reflexes in quadriceps (Q), hamstring (Ham), tibialis anterior (TA) and triceps surae (TS) of an individual with incomplete spinal cord injury classified as AIS C. Obtained by transcutaneous lumbar spinal cord stimulation with 0.2 Hz stimulating pulse frequency. (Minassian, et al., 2012a)

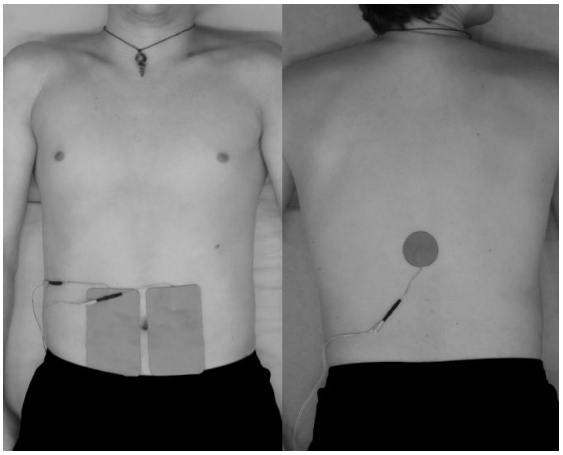

Figure 7 – Placement of stimulating electrodes for tSCS at T11-T12 level

The posterior roots can be activated by both epidural and transcutaneous electrical stimulation. With epidural spinal cord stimulation, the active electrode is implanted into the epidural space over the T11-T12 vertebral level, corresponding to the spinal cord entry points of lumbar spinal nerves projecting to quadriceps, hamstrings, tibialis anterior and triceps surae. Transcutaneous stimulation (tSCS) provides a non-invasive alternative: the active electrodes are placed over the paravertebral skin at T11-T12 level, larger counter electrodes are fixated to the lower abdomen (Figure 7). This can selectively target the posterior roots of L2-S2 spinal nerves despite the relatively large distance to the electrodes and the diffuse electric field (Minassian, et al., 2012a), as a result of the non-uniformities of the excitation thresholds of the axons along their trajectories as well as the differing electrical conductivities of anatomic structures.

Neurons can be artificially excited by depolarizing their membrane above the activation threshold to generate an AP, with the lowest threshold at the nodes of Ranvier, compared to the dendrites and soma (Porter, 1963; Nowak & Bullier, 1998; Rattay, 1998; Rattay, 1999). Larger axon diameter and myelinization decrease the threshold of the electrode current (Ranck, 1975; Rattay, 1987; Rattay, 1990; Roth,

1994). Furthermore, the activating function concept (Rattay, 1998; Rattay, 1999) predicts sites of lowest activation thresholds of the axon as the second spatial derivative of the external potential along its trajectory. Within the diffuse electrical field of transcutaneous stimulation, changes of the external field along the neuronal membrane occur at axonal bends and changes of the electrical conductivities in the anatomy along the axonal path. Using cathodic stimulation, modeling studies (Rattay, et al., 2000; Ladenbauer, et al., 2010; Danner, et al., 2011; Danner, et al., 2014) have identified the sites of lowest activation threshold as the posterior roots near their entry point into the spinal cord, especially in the largest diameter Ia afferents, which are also closest to the dorsal stimulating electrode (Rattay, 1990). As a consequence of the length disparity of spinal cord and spinal column, both posterior and anterior lumbar roots exhibit sharp bends near the spinal cord, though the orientation of the anterior root relative to the electric field results in a negative second derivative and therefore an increased threshold for cathodic stimulation, while that of the posterior root is lowered. Additionally, the change of surrounding tissue from the highly conductive cerebrospinal fluid (1.7 S/m (Holsheimer, 1998b; Rattay, et al., 2000)) to the less conductive transversal (0.083 S/m) (Holsheimer, 1998b; Rattay, et al., 2000) and longitudinal (0.6 S/m) (Struijk, et al., 1991; Struijk, et al., 1992; Struijk, et al., 1993) white matter further decreases this threshold. Anterior roots have been predicted to have their lowest threshold at their exit from the spinal column. Longitudinal fibers on the other hand, especially the posterior column located closest to the stimulating electrode, don't have sufficiently high electric field changes along their trajectories, resulting in almost no lowered threshold sites (Danner, et al., 2011).

Since the currents in the body are predominantly conductive currents (Schwan & Kay, 1957), the body can be viewed as a resistive volume conductor, described by Ohm's law as $\vec{J} = \gamma\vec{E}$ (γ = electric conductivity). This means that successful activation of

posterior roots depends on the transversal current that can pass through the vertebral canal, as pictured in Figure 8. In a computational model (Ladenbauer, 2008), current has been shown to mainly enter through the spaces between the spinous processes containing the intervertebral disks and ligaments because of the high difference of electric conductivity between vertebral bone (0.02 S/m (Szava, 2006)) and disks (0.6 S/m (Gu, et al., 2002; Szava, 2006)).

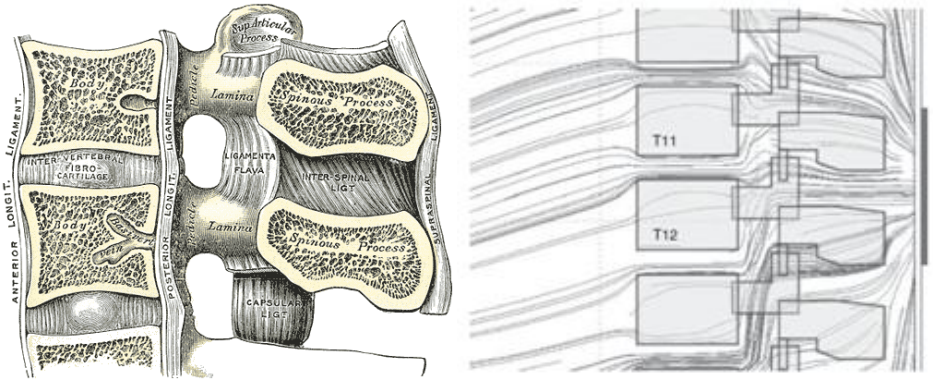

Figure 8 – Left: Sagittal plane cross section of spinal column; the ligaments and intervertebral disks have significantly higher electric conductivities (Wikipedia, 2015). Right: Computer simulation of current density through vertebral canal; only bones and the dorsal stimulating electrode are depicted, line density corresponds to current density (Danner, et al., 2011).

The current density distribution within the spinal canal, where the lowest activation threshold sites of the targeted neural structures are, is therefore dependent on the geometry of spinous processes and intervertebral disks, which could influence tSCS efficacy for different spinal curvatures. Many electrophysiological studies using tSCS, where subjects' positions varied from supine (Minassian, et al., 2007b) and seated (Roy, et al., 2012) to walking (Courtine, et al., 2007), have been recently performed, with varying results. A sitting position has been found to provide better reflex recruitment at L1-L3 instead of T11-T12 like it has been observed in standing and supine positions. Prone positions resulted in predominant excitation of the anterior roots and thus direct motoneuron stimulation (Knikou, 2013; Danner, et al.,

submitted). This indicates altered activation threshold sites that could be caused by geometrical changes of the spinal cord and canal. Gravitational migration of the spinal cord within the cerebrospinal fluid of the epidural space (Holsheimer, et al., 1994) and the resulting differences in spinal root trajectories (Rattay, 1999) could be a reason for this, differences between standing and supine positions could also be attributed to reflex pathway modifications (Hayashi, et al., 1992). The role that spinal curvature could play in postural tSCS efficacy disparities has not been studied yet.

2.5. The Hoffmann reflex

In contrast to lumbar SCS, the Hoffmann reflex or H reflex is elicited at the mixed peripheral nerve. It is widely used to study the spinal motoneuron excitability through stimulation of Ia primary afferents that monosynaptically project to the homonymous motoneurons, as shown in Figure 9. Soleus, quadriceps and flexor carpi radialis are commonly used for H reflex studies, while elicitation in the tibialis anterior, for example, is difficult to achieve. Generally, stimulation is possible for any muscle whose parental nerve can be accessed (Pierrot-Deseilligny & Burke, 2012).

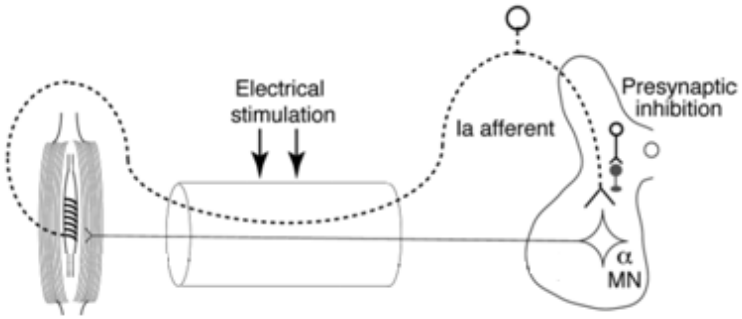

Figure 9 – Pathway of monosynaptic H reflex arc (slightly adapted from (Pierrot-Deseilligny & Burke, 2012))

At the spinal level, the volley of the Ia afferent produces EPSPs in multiple motoneurons. Smaller, slower motoneurons produce larger ESPS for a fixed afferent

volley, which results in a recruitment order similar to the physiological order: slower motor units are activated first, faster ones only with larger inputs. Direct stimulation of motor fibers, on the other hand, follows an inverse recruitment order, since large-diameter fibers are more readily exited by a given stimulus. In mixed peripheral nerve stimulation, the largest afferent fibers are therefore excited first, followed by large motoneurons. Additionally, electric stimulation of a nerve produces a bidirectional volley; the orthodromic volley follows the physiologic direction, while the antidromic volley propagates along the opposite direction. This results in the recruitment curve for the H reflex shown in Figure 10. At low intensities, only the Ia fibers are activated, which in turn elicit motor volleys in small motoneurons. Increasing the stimulus intensity results in direct activation of large motoneurons and thus an M wave, characterized by a significantly shorter latency compared to the H reflex since the additional distance to the spinal cord as well as synaptic transmission are omitted, while the H reflex increases with the number of indirectly, trans-synaptically activated motoneurons because of the increase of Ia volley amplitude. At the descending portion of the H curve, the stimulus is big enough to reach medium diameter motoneurons directly as well as indirectly. Since direct activation of motoneurons also produces an antidromic volley, the reflex response of these motoneurons is eliminated by collision with the antidromic volley. These motoneurons only contribute to the M wave of the recorded compound muscle action potential (CMAP), therefore the H reflex amplitude decreases while the M wave increases, until the H reflex is completely suppressed by collision in all recruited motoneurons, while the M wave reaches its maximum when all motor fibers are directly activated.

This means that stimulation intensities on the descending limb of the H curve are not suitable for assessing facilitation or inhibition of the H reflex with changing motoneuron pool excitability since the recorded H reflex does no longer reflect the

number of trans-synaptically activated motoneurons. Therefore, it is recommended to operate on the ascending limb of the H curve (Knikou, 2008; Pierrot-Deseilligny & Burke, 2012).

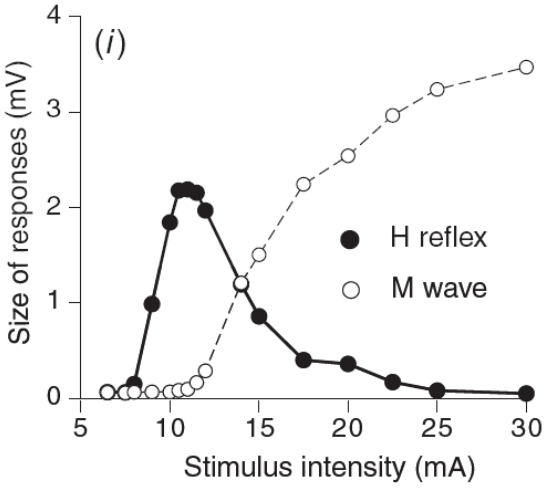

Figure 10 – Recruitment curve of H reflex and M wave for soleus. (Pierrot-Deseilligny & Burke, 2012)

2.6. Comparison of PRM and H reflex

In conclusion, the PRM reflex gain can be influenced by two factors: First, biophysical changes like the curvature of the spinal column because of altered current density distributions or the geometry of the spinal cord within the spinal canal and corresponding spinal root trajectories for different subject positions, and secondly, a modification of the reflex pathway by Ia, Ib and II afferents or corticospinal and vestibular inputs. In contrast, the H reflex is not influenced by the biophysical changes of the spinal cord and its surroundings. Assuming steady stimulation conditions, signified by a constant M wave, the H reflex gain on the ascending limb of the recruitment curve is only dependent on the central state. While H and PRM reflex are not the same, they share certain similarities: they are both elicited by stimulating afferents with large diameters, mainly Ia fibers, and, at low frequencies, they both

activate α-motoneurons monosynaptically. Therefore, to exclude central state influences and only study the biophysical dependencies of PRM efficacy, the H reflex can be elicited in a muscle where the PRM reflex is measured as well.

During SCS, though, multiple spinal roots of many lower limb muscle groups are activated simultaneously, in contrast to peripheral nerve stimulation. The soleus's response to SCS, for example, reflects the excitation of the soleus's motoneuron pool by soleus afferents as well as the concurrently activated tibialis anterior, quadriceps, and other possible synergists or antagonists. Therefore, when comparing H reflex and PRM reflex of the same muscle, quantification is not feasible. If the H reflex is kept constant, though, changes of the PRM reflex CMAP can be attributed to biophysical, rather than central state excitability changes. This is, strictly speaking, only valid for the muscle where the H reflex is also elicited, since other muscles' reflex pathways could still be modified at a spinal level.

3. Methods

To study the effects of the spinal curvature on PRM reflex gain, tSCS was administered to able-bodied subjects in different positions (supine, lateral, sitting and standing) and spinal curvatures (neutral, maximal dorsal flexion, maximal ventral flexion). Curvatures were measured across four different positions to ensure the observed effects were not merely a position specific phenomenon that could solely be attributed to gravitational subsidence of the spinal cord or change in its craniocaudal position within the spinal canal. To exclude central state influences on the reflex gain, the H reflex was also measured for every position and spinal curvature, and kept constant by adjusting body position, especially knee and hip angle, before spinal stimulation. Therefore, the main target value to determine the effect of the spinal curvature was the peak to peak amplitude of the CMAP of the soleus where the H reflex was elicited as well. The soleus, rather than gastrocnemius, was chosen because, while the two gastrocnemius heads are both ankle extensors and knee flexors, the soleus is only an ankle extensor, so its muscle and tendon tonus can be kept relatively constant throughout the measurement with an ankle orthesis. To control for direct motor activation, double pulses were used along with single pulses, to check for post-activation depression. For brevity, the peripheral H reflex stimulation will be referred to as PS from here on.

3.1. Subjects

Ten neurologically healthy subjects (3 female, 7 male) between the ages of 18-40 participated in the study. Prior to the measurement, all participants signed an informed consent form and the women underwent a pregnancy test in order to rule out pregnant subjects. Further exclusion criteria included spinal, cranial or abdominal surgeries, meningitis, primary muscular diseases, as well as pronounced postural

anomalies or restricted flexibility of the lower limbs. The study was approved by the institutional review board of the Medical University of Vienna.

3.2. Stimulation and Recording Setup

Both tSCS and PS were performed with a CE-certified constant current stimulator (Stimulette r2x, Fa. Schuhfried Medizintechnik, Vienna) using rectangular, 1 ms long pulses. To clean the skin and ensure uniform, high conductivity, an alcohol-based electrode spray was applied to the skin and the stimulation electrodes.

For tSCS, the cathode was a 5 cm diameter self-adhesive electrode (STIMEX, schwa-medico, Ehringhausen, Germany), placed midline on the skin between the T11 and T12 spinous processes. This position was subsequently adjusted until quadriceps and soleus responses had the same intensity threshold. The anode consisted of two interconnected 13x8 cm self-adhesive electrodes (STIMEX, schwa-medico, Ehringhausen, Germany), placed horizontally directly above and below the umbilicus. While longitudinal placement to both sides of the umbilicus is more widely used, the electrodes tended to detach during sitting positions with ventral flexion of the spine.

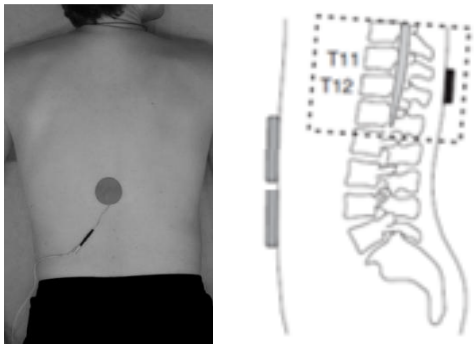

Figure 11 – Electrode placement for tSCS; cathode - one 5 cm diameter electrode placed over skin between T11 and T12 spinous processes, anode - two connected rectangular 13x8 cm anodes above and below umbilical. (right: (Minassian, et al., 2012a), adapted)

The H reflex was elicited by N. tibialis posterior stimulation in the left soleus, whose peak to peak amplitude of the CMAP were used as the main target value in assessing the effect of the spinal curvature on tSCS efficacy. The anode was placed proximal of the patella (5x6.5 cm, STIMEX, schwa-medico, Ehringhausen, Germany). A suitable site for the cathode within the popliteal fossa was determined with a hand held stimulation probe, to avoid direct stimulation of the deep peroneal nerve innervating the tibialis anterior and find a position with adequate M wave and H reflex amplitudes. Since the M wave was needed to ensure the number of stimulated axons by the electrical stimulation remains the same during postural changes and gain of the H reflex pathway can only accurately be observed at the ascending limb of its recruitment curve, it was critical for this study to elicit an M wave while still in the dynamic range of the ascending H reflex curve. Therefore, subjects in whom M waves could only be measured when the H reflex was already at its peak or on the descendant limb were excluded from the study. When a suitable cathode site was found, an ECG electrode (self-adhesive, SKINTACT, Leonhard Lang GmbH, Austria) was affixed to it. To reduce movement of the cathode, a folded tissue was pressed against it and the knee was wrapped with a bandage, with care taken to maintain sufficient knee flexibility and normal blood circulation.

The stimulus-evoked electromyographic activity was recorded by pairs of monopolar Ag/AgCl surface electrodes placed bilaterally on rectus femoris, hamstring, tibialis anterior and soleus. They were attached with 3 cm interelectrode distance along the midline over the muscle belly. For the soleus, the placement was 3 cm and 6 cm respectively below the joiningof the gastrocnemius medial and lateralis heads into the Achilles tendon, to avoid recordings of gastrocnemius activity. The skin was prepared by rubbing off the outmost skin layer with an abrasive paste to reduce skin impedance. Additionally, electrode gel was used. Total impedance was kept below 10 kΩ and 20 kΩ for both solei and all other muscles, respectively.

The reference electrodes, one monopolar EMG electrode for each leg, were placed above the lateral malleolus, where no muscles activity would be recorded. Another pair of EMG electrodes was placed horizontally at the waist, approximately at the L2-L3 spinal level with an interelectrode distance of 5 cm, to record the tSCS artefact to trigger signal recording. The PS recordings were triggered by the stimulation artefact at the soleus.

All electrodes were fixated with tape to avoid detachment during postural changes.

3.3. Positions

Throughout the measurement, all eight muscles were screened for background muscle activity to ensure the subjects were relaxed. The neck was always in straight extension of the spine and the head neutral in relation to the neck. Maximal dorsal and ventral flexion of the spine was defined as the maximal flexion the subject could comfortably accomplish while still relaxed. Positioning was facilitated by pillows and folded bed linens, and kept as constant as possible across subjects.

In the supine position, the neutral spinal curvature had subjects lying flat on their backs with a pillow underneath their head to keep their neck straight with arms relaxed and to their sides. For dorsal flexion, a pillow was placed under the T11-T12 level of the spine, while the hips and shoulders remained comfortably on the bed. During ventral flexion, pillows were placed under the shoulders and head. For the lateral position, a pillow was placed under the head, a folded bed linen under the waist to ensure a straight spine within the frontal plane, and the arms were curled up in front of them. Subjects were lying on the side of the main soleus, where the H reflex was elicited, since it was observed that the upper leg sometimes exhibited highly suppressed PRM reflex responses, regardless of spinal curvature. A pillow was placed between the knees to keep the upper leg straight in the frontal plane and keep it from pinning down the bottom leg too much. In the sitting position, the arms

were kept relaxed at the subjects' sides, and the neutral spinal curvature was defined as sitting up straight, the shoulders in a vertical line with the hips. During standing, both ankle ortheses were removed to facilitate relaxed standing, since the ground contact ensured a relatively constant ankle joint angle. Neutral curvature was again defined as shoulders over hips, arms were kept relaxed.

3.4. Measuring Protocol

The measurement was started in the supine neutral position, with both ankles fixated at approximately 90° by the ortheses. The suitable PS and tSCS sites were determined and not changed for the rest of the measurement.

All pulses were rectangular, biphasic, cathodic constant current pulses with a duration of 1 ms per phase. For double pulses, the interstimulus interval was 35 ms. All measurements were repeated six times. For PS, only single pulses were used, repeated six times, with a pause of at least 8 s between repetitions. During tSCS measurements, every second one was a double pulse. After the subject had moved or background muscle activity was observed, measurements were only resumed after at least 20 s. The maximum stimulation intensity was 125 mA.

M_{MAX}, the maximal obtainable amplitude of the M wave during PS, was averaged out of six repetitions and subsequently used for determining the stimulation intensities: the intensity for tSCS (I_{tSCS}) was the intensity where the peak to peak amplitude of the main soleus (A_{tSCS}) was 50 % of M_{MAX}, for PS, I_H should elicit an H reflex peak to peak amplitude (A_H) of 25 % of M_{MAX}, while on the ascending limb of the recruitment curve. If A_{tSCS} was already saturated at 50 % of M_{MAX}, I_{tSCS} was chosen as the intensity where A_{tSCS} was 50 % of the maximum main soleus amplitude. Mean value and standard deviation of A_{tSCS} - relative to 50% of M_{MAX} - were 1.02 ± 0.20 , 0.9 ± 0.32, 0.79 ± 0.34 and 0.80 ± 0.24 for the neutral curvature during supine, lateral, sitting and standing positions, respectively.

Then, PS with I_H was performed, still in the supine neutral position, and the average of A_H and M wave amplitude (A_M) was recorded. Then, tSCS with I_{tSCS} was measured. Afterwards, PS was tested in the supine dorsiflexion position. First, A_M was adjusted to the value previously measured for neutral spinal curvature (acceptable range ± 25 %) by adjusting I_H to ensure that approximately the same number of motoneurons was accessed. At this new I_H, the subject's position was adjusted until A_H was also in the range of ± 25 % of the supine neutral position. Then, with the subject remaining as still as possible, PRM reflexes were measured with the same I_{tSCS} as used in the neutral position. For the supine ventralflexion position, A_M and A_H were again compared to neutral spinal curvature values to adjust I_H, while I_{tSCS} was kept the same.

Afterwards, the next position, standing, was measured. New suitable I_{tSCS} and I_H were determined according to the guidelines described above. In total, the order of the measured positions was

- Supine, neutral spinal curvature
    - Dorsiflexion
    - Ventralflexion
- Lateral, neutral
    - Dorsiflexion
    - Ventralflexion.
- Standing, neutral
    - Dorsiflexion
    - Ventralflexion
- Sitting, neutral
    - Dorsiflexion
    - Ventralflexion

3.5. Data Acquisition and Processing

The EMG signals were amplified 600 fold, by a custom-built amplifier, filtered to a 10-600 Hz bandwidth and subsequently digitized at 10 kHz with a USB-NI 6261 data

acquisition card (National Instruments Inc., Austin, TX, USA). They were recorded with DasyLab 12.0 (Measurement Computing Corporation, Norton, MA; USA), with a time window of 100 ms pre-trigger and 900 ms post-trigger, and processed with MATLAB (Release 2013b, MathWorks, Inc., Natick, MA, USA).

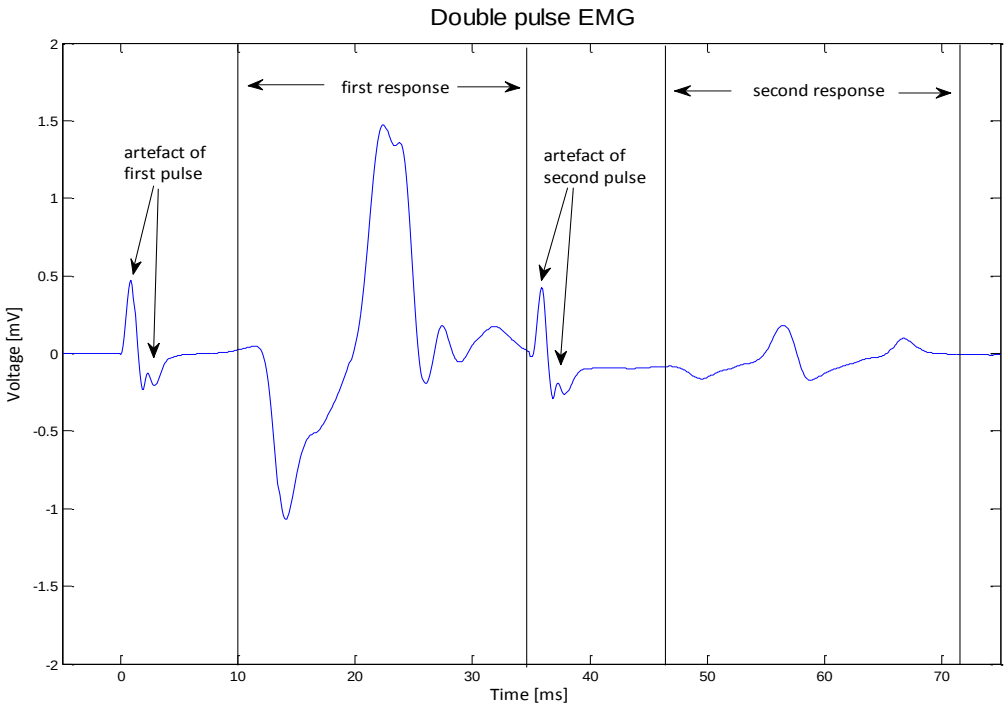

Figure 12 – EMG of muscle response to one double pulse with 35 ms ISI; artefacts of the two stimulation pulses, followed by the response CMAP to each stimulation, are shown. A_1 was calculated from the average of the peak to peak amplitudes of first responses, A_2 from second response.(Obtained from hamstring in supine position with spinal dorsiflexion.)

Figure 12 shows an EMG response to a double pulse. The two parameters used to characterize tSCS efficacy were the peak to peak amplitude of the first response (A_1) and the ratio of the peak to peak amplitudes of second to first response (A_2/A_1). For A_1 calculation, the peak to peak amplitudes of responses from the three single pulses as well as the first responses from the three double pulses were measured and averaged. A_2 was obtained in a similar fashion, from the second responses of the

three double pulses. H and M wave amplitudes were also calculated from the average of all six pulses. For A_2/A_1 analysis, measurements with $A_1 < 0.1$ mV were excluded.

3.6. Statistic Analysis

The data was analyzed with SPSS Statistics (IBM Corp., Version 23 for Windows) with a generalized linear mixed model (GLMM; Table 1). For A_1 analysis of the main soleus, the Hessian matrix used for computing the estimated covariance matrix was not positive definite and the model could not be calculated. In this case, the variance contribution of the body position to overall data variance was found to be too small ($3.4 \cdot 10^{-14}$), a common cause of these types of errors (Grace-Martin, 2015), and therefore body position as a random effect was excluded from A_1 analysis of the main soleus without significantly impacting the model validity, since positions could not account for any data variation. Covariance matrix types were selected to minimize the Bayesian Information Criterion. The fit of all models was controlled by inspection of the histogram of Pearson residuals. An alpha error of $p < .05$ was regarded as significant. Post-hoc tests were pairwise comparisons of the estimated marginal means with sequential Bonferroni adjustment for multiple comparisons at significance level .05.

Table 1 – GLMM Parameters

	Main soleus analysis	**All muscles analysis**
Target	A1 or A2/A1 ratio	A1 or A2/A1 ratio
Probability distribution	Normal	Normal
Link function	Identity	Identity
Covariance matrix type	Scaled identity	First-order autoregressive
Subjects	Subject	Subjects*Legside
Repeated measures	Curvature*Position	Muscle*Curvature*Position

Fixed effects	Curvature Curvature*Position	Curvature Curvature*Position Muscle Muscle*Curvature Muscle*Position Muscle*Curvature*Position
Random effect	Only for A_2/A_1 analysis: Position, with intercepts Subject combination: Subject	Position, with intercepts Subject combination: Subject*Legside
Random effect covariance type	Scaled identity	Scaled identity
Post-estimation confidence level	95%	95%
Post-estimation degree of freedom	Satterthwaite approximation	Satterthwaite approximation
Post-estimation covariances	Model-based	Model-based
Adjustment for multiple comparisons	Sequential Bonferroni, significance level .05	Sequential Bonferroni, significance level .05

4. Results

Table 2 shows the data excluded from the analysis because of M wave or H reflex values outside the ± 25 % range of the neutral spinal curvature, or because no data could be obtained (one case, in lateral and standing position, where no muscle responses could be elicited at maximal stimulation intensities).

Table 2 – Number of measurements out of 10 Subjects that were excluded from further analysis.

	Supine	Lateral	Sitting	Standing	
Dorsiflexion	2	3	2	4	**=11**
Ventralflexion	4	3	2	4	**=13**

4.1. Main soleus

Figure 13 shows typical main soleus responses, obtained from one subject. A complete absence of responses during ventralflexion occurred, though not always in the same positions across subjects. Second responses were rarely observed.

First response amplitudes

The generalized linear mixed model of the amplitudes of first responses revealed a highly significant effect of spinal curvature on first-response amplitude, $F(2,78) = 29.322$, $p < .001$ (Figure 14A). Post-hoc tests showed that amplitudes for ventralflexion were significantly lower compared to neutral curvature, $t(78) = 7.293$, $p < .001$, or dorsiflexion, $t(78) = 5.896$, $p < .001$, while neutral curvature and dorsiflexion did not differ, $t(78) = 1.185$, $p = .240$.

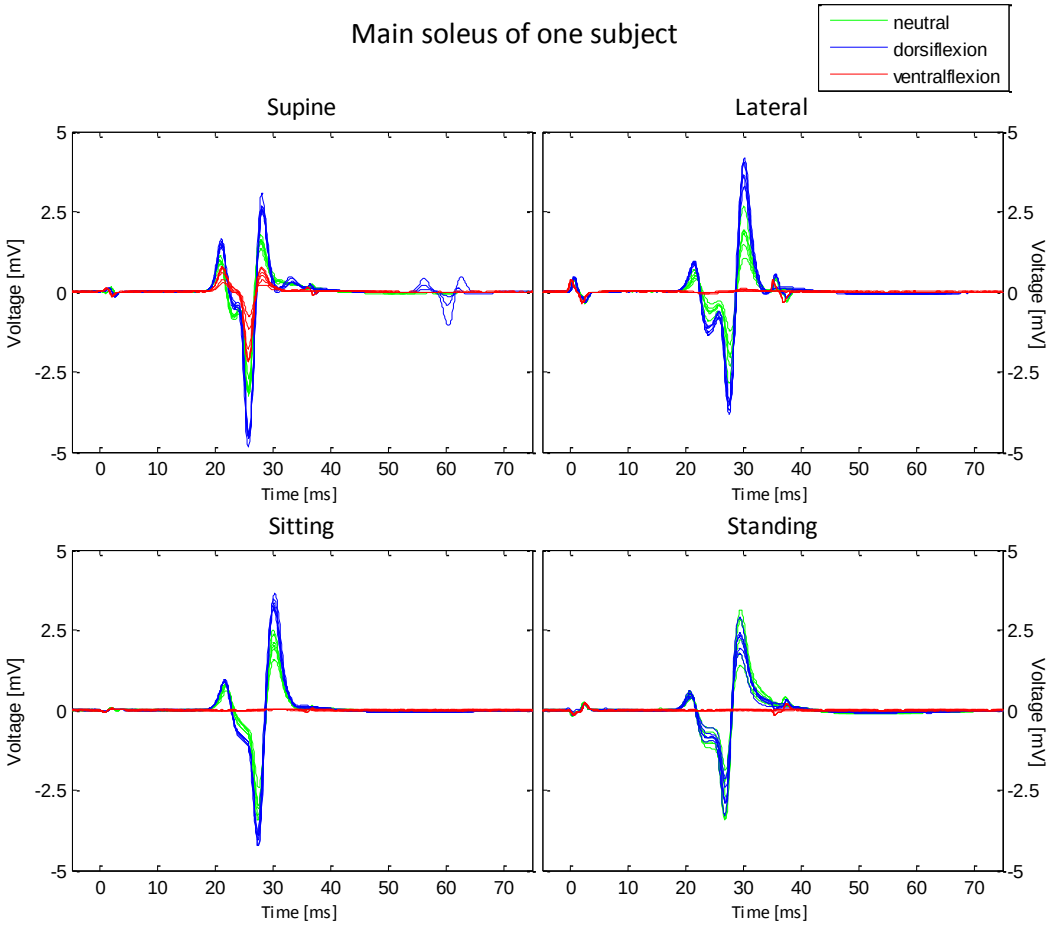

Figure 13 – Main soleus EMG of one subject for all positions and curvatures, all six pulses for each position and curvature are displayed. Spinal ventralflexion resulted in smaller or no reflex responses.

The interaction effect between curvature and position was not significant, $F(9,78) = .868$, $p = .557$, indicating that the effect of curvature did not vary across different body positions. To investigate whether the curvature-amplitude relation was present in all positions, pairwise contrasts with a sequential Bonferroni adjustment for multiple comparisons were performed. They revealed significantly (all $p < .015$) lowered amplitudes for ventralflexion compared to neutral curvature or dorsiflexion for all positions except standing, where, while comparison of ventralflexion to neutral

curvature did yield significant results, $t(78) = 3.342$, $p = .005$, ventralflexion to dorsiflexion was narrowly above significance level, $t(78) = 2.198$, $p = .062$. Again, comparison of dorsiflexion to neutral curvature did not reveal any significant amplitude differences in any position (all $p > .14$). The marginal means of each position are shown in Figure 14B.

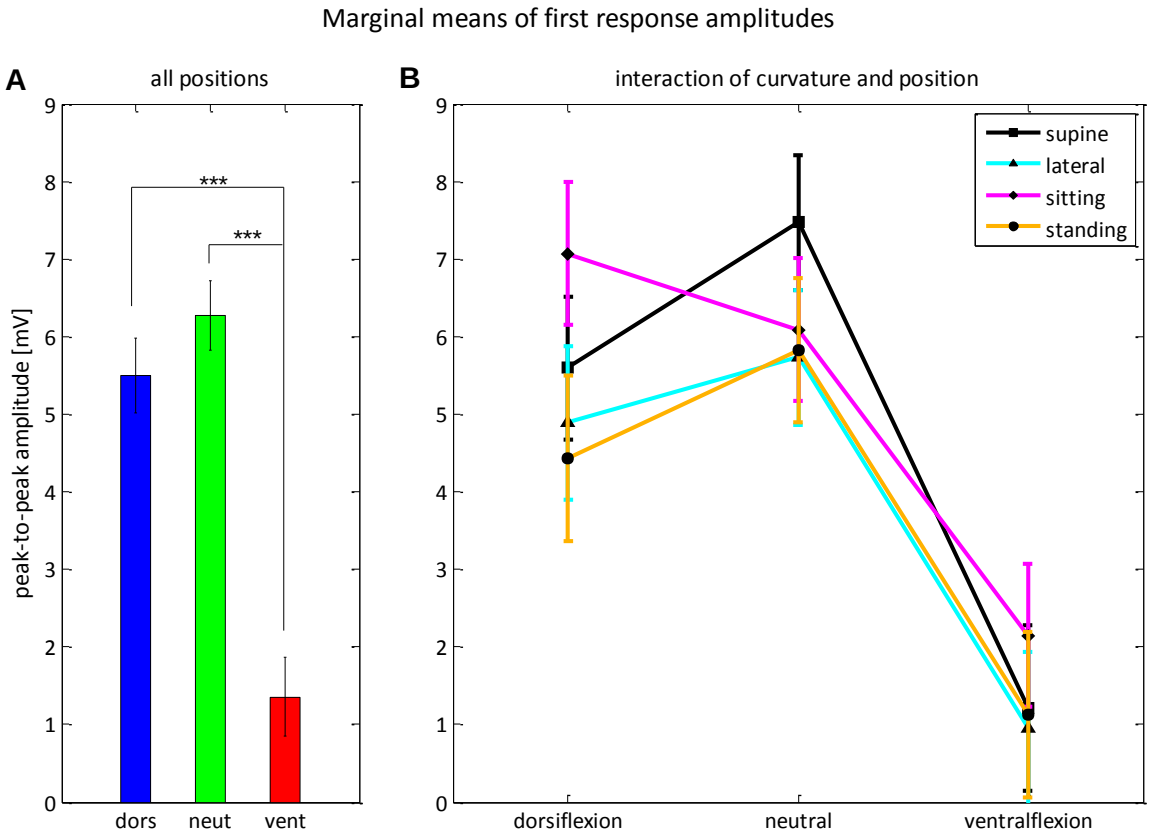

Figure 14 – Model estimates of marginal means and standard errors of first amplitudes for each spinal curvature in the main soleus, across all positions (A) and for individual positions (B). Brackets indicate significant differences (***: $p < .001$). Ventralflexion shows a significant amplitude decrease in all positions.

Ratio of second to the first response amplitude

For the analysis of A_2/A_1ratio changes across spinal curvatures, 19 ventralflexion, 1 dorsiflexion and no neutral curvature measurements were excluded because their first response amplitudes were below 0.1 mV.

The generalized linear mixed model showed that spinal curvature was a significant effect for the ratio of second to first response amplitudes, $F(2,44) = 6.430$, $p = .004$ (Figure 15A). Pairwise post-hoc tests revealed significantly higher A_2/A_1 ratios for ventralflexion compared to neutral curvature, $t(45) = 3.425$, $p = .004$, or dorsiflexion, $t(46) = 3.208$, $p = .005$, while dorsiflexion did not result in any changes of A_2/A_1 compared to neutral spinal curvature, $t(42) = .013$, $p = .990$.

The interaction effect of position and curvature was not significant, $F(9,45) = .998$, $p = .456$, suggesting that effects of curvature on A_2/A_1 ratios did not vary between different positions. Again, to investigate whether significant differences between curvatures occurred in individual positions, pairwise contrasts with sequential Bonferroni adjustment for multiple comparisons were performed. They showed significant A_2/A_1 changes during standing for ventralflexion compared to both neutral curvature, $t(43) = 3.304$, $p = .006$, and dorsiflexion, $t(45) = 3.059$, $p = .007$. For lateral and sitting positions, barely significant changes occurred for only one pairwise comparison (lateral: neutral to ventralflexion, $t(42) = 2.784$, $p = .024$, sitting: dorsi- to ventralflexion, $t(42) = 2.501$, $p = .049$). Finally, in the supine position, contrasts revealed no changes of A_2/A_1 for different curvatures. As always, no significant differences between dorsiflexion and neutral curvature were found in any position (all $p > .45$). Figure 15B shows the A_2/A_1 ratios for each position.

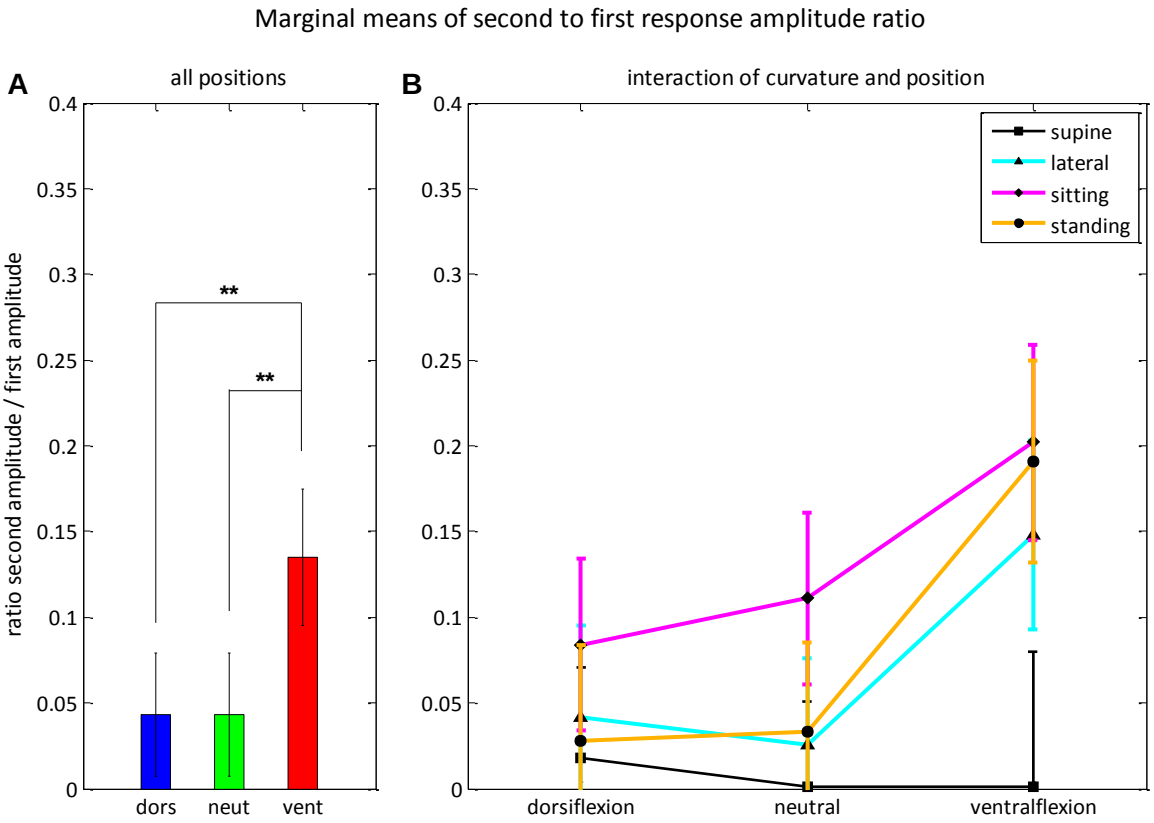

Figure 15 – Model estimates of marginal means and standard errors of A_2/A_1 ratios for each spinal curvature in the main soleus, across all positions (A) and for individual positions (B). Brackets indicate significant differences (**: $p < .01$). Ventralflexion resulted in significantly increased ratios overall, most pronounced during standing, to a lesser extent during lateral lying and sitting, while for supine positions, no significant differences were found. Note that supine ratios were smallest overall.

4.2. All Muscles

Figure 16 depicts responses of all left leg muscles of one subject to spinal curvature, obtained during sitting. Soleus has the highest amplitudes, followed by hamstrings. Ventralflexion again resulted in a diminished amplitude, except in quadriceps. Second responses most frequently occurred in the quadriceps, with 97.6 % of all A_2/A_1 ratios above median ratio of all muscles.

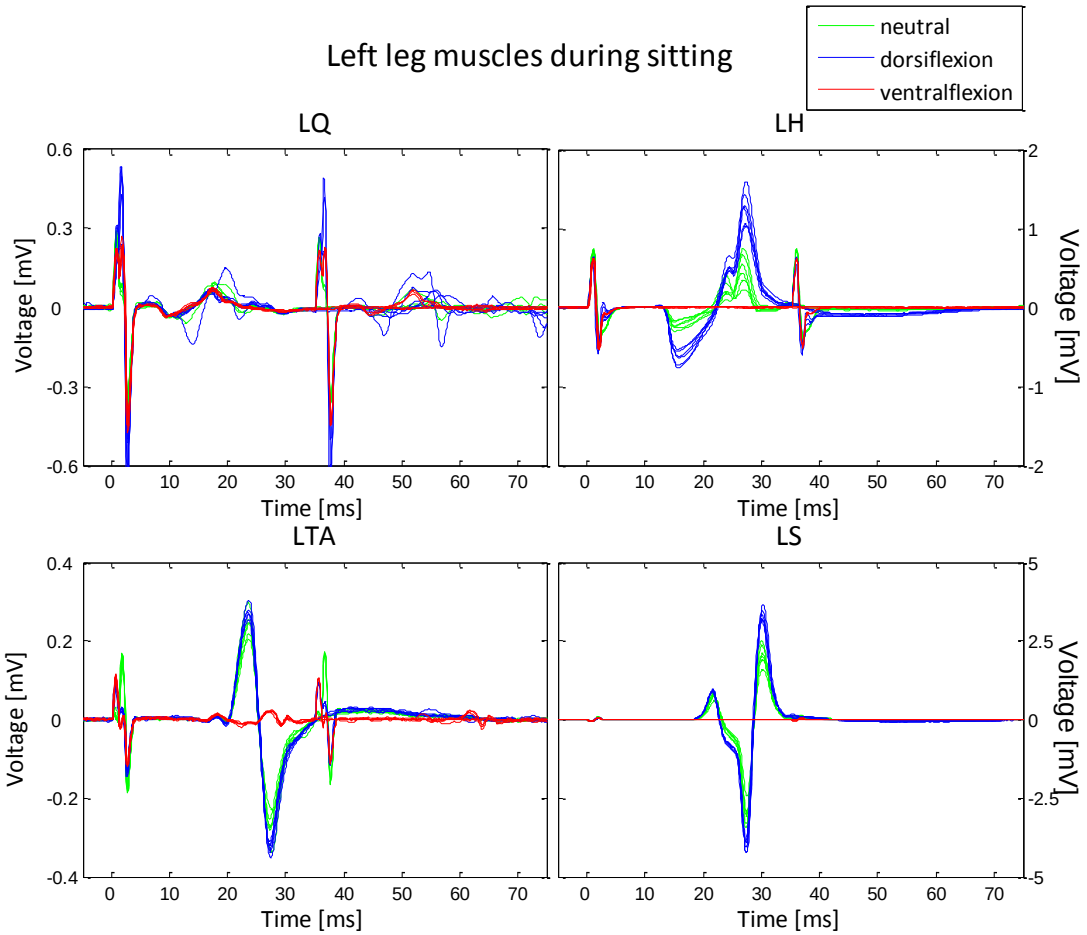

Figure 16 – Left leg muscles of one subject while sitting, six repeated stimulation pulses per curvature. Ventralflexion resulted in a decreased first response amplitude, especially in hamstrings and soleus.

First response amplitude

The generalized linear mixed model of the first response amplitudes showed a highly significant effect of the curvature on first amplitudes, $F(2,339) = 32.487$, $p < .001$. Post-hoc tests revealed that ventralflexion yielded a highly significant decrease of first responses in comparison to neutral curvature, $t(326) = 7.749$, $p < .001$, and dorsiflexion, $t(356) = 6.093$, $p < .001$, while dorsiflexion and neutral curvature did not

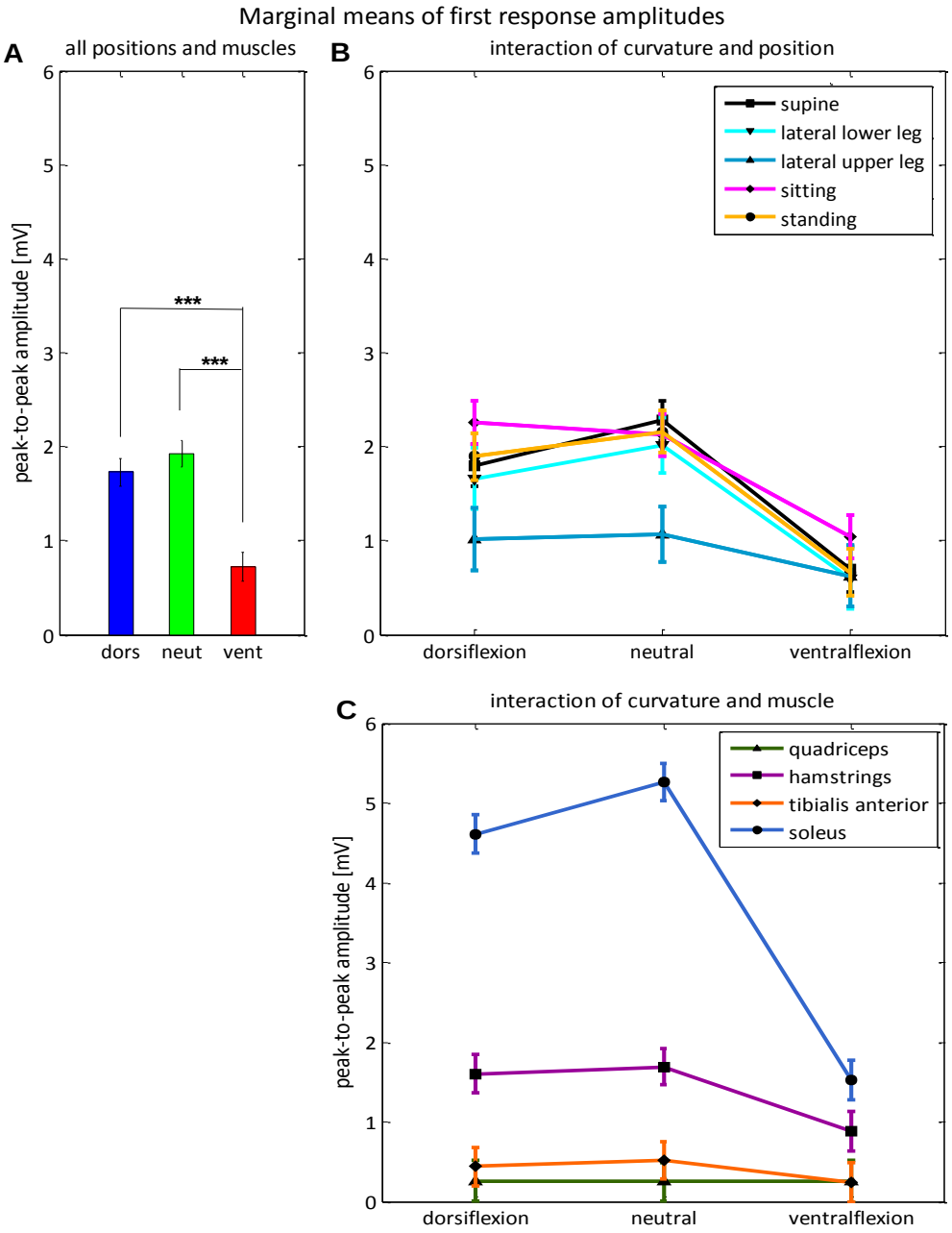

Figure 17 – Model estimates of marginal means and standard errors of first response amplitudes for each spinal curvature, across all positions and muscle groups (A), for each positions across all muscle groups (B) and for each muscle group across all positions (C). Brackets indicate significant differences (***: $p < .001$). Ventralflexion shows a significant amplitude decrease in each position except in the upper leg during lateral positions, but only in soleus and to a lesser extent in the hamstrings, while quadriceps and tibialis anterior showed no changes in first response amplitudes upon changed spinal curvature.

differ significantly, t (338) = 1.330, p = .184. Figure 17A depicts the marginal means and standard errors of the first response amplitude.

The effect of muscle group on first response amplitude was highly significant, F (3,194) = 151.449, p < .001, reflecting the varying recorded CMAP amplitudes for different muscles. The interaction effect of muscle and position was highly significant as well, F (12,436) = 4.755, p < .001.

The interaction effect of curvature and muscle was also highly significant, F (6,297) = 17.006, p < .001, indicating that the relation between curvature and A_1 was not consistent across all muscle groups. Post-hoc tests revealed that a dependence of amplitude on spinal curvature was not present in quadriceps (all p = 1) and tibialis anterior (all p = 1), while the soleus showed highly significant changes between ventralflexion and neutral curvature, t (319) = 3.743, p < .001, and dorsiflexion, t (273) = 3.087, p < .001, and the hamstrings a significant difference between ventralflexion and neutral curvature, t (318) = .812, p = .024, and a barely not significant difference between ventral- and dorsiflexion, t (269) = .721, p = .054. Marginal means of A_1 for curvatures in each muscle group are depicted in Figure 17C.

The interaction effect of curvature and position, on the other hand, was not significant, F (8,466) = 1.242, p = .273, suggesting that the relation between curvature and first response amplitude was the same across all positions. To investigate whether there were significant differences between curvatures in each individual position, pairwise contrasts with a sequential Bonferroni adjustment for multiple comparisons were performed. They revealed highly significant differences (all p < .001) of ventralflexion to both neutral curvature and dorsiflexion, in all but the lateral positions, where upper and lower leg were analyzed separately. In the lower leg significant differences of ventralflexion to neutral curvature, t (607) = 1.418, p < .001, and dorsiflexion, t (634) = 1.063, p = .013, were present, while the upper leg

showed no significant changes (both $p > .636$). Again, differences between neutral curvature and dorsiflexion were not observed (all $p > .30$) except the supine position, $t(556) = .480$, $p = .048$. Figure 17B depicts the marginal means and standard errors for each position and curvature.

The interaction effect of curvature, muscle and position was not significant, $F(24,440) = 1.112$, $p = .326$.

Ratio of second to first response amplitude

For the analysis of A_2/A_1 ratios, 120 ventralflexion, 40 dorsiflexion and 33 neutral curvature measurements were excluded because A_1 was below 0.1 mV, with 74 of those from quadriceps, 29 from hamstrings, 49 from tibialis anterior and 41 from soleus.

The generalized linear mixed model of the ratios of second to first response amplitude yielded a highly significant effect of spinal curvature on the A_2/A_1 ratios, $F(2,320) = 12.761$, $p < .001$ (Figure 18A). Post-hoc tests revealed highly significant increases of A_2/A_1 during ventralflexion compared to neutral curvature, $t(343) = 4.468$, $p < .001$, and dorsiflexion, $t(327) = 4.638$, $p < .001$, while neutral curvature and dorsiflexion did not differ significantly, $t(299) = .433$, $p = .665$.

There was a highly significant effect of muscle group on the A_2/A_1 ratio, $F(3,100) = 41.142$, $p < .001$, with post-hoc tests revealing significant differences between all of them. Quadriceps had the highest A_2/A_1 ratios, followed by tibialis anterior, hamstrings and soleus.

The interaction effect of muscle and position was also highly significant, $F(12,307) = 3.206$, $p < .001$, indicating that these muscle group differences varied across positions.

The interaction effect of muscle and curvature was not significant, $F(6,242) = .840$, $p = .540$, suggesting that the increase of A_2/A_1 ratio from neutral curvature or dorsiflexion to ventralflexion did not differ significantly across muscle groups. Marginal means of A_2/A_1 ratios of single muscle groups for all curvatures are depicted in Figure 18C.

The interaction of curvature and position was significant, $F(8,338) = 3.510$, $p = .001$, indicating that the dependence of A_2/A_1 ratio on spinal curvature differed across positions. Post-hoc tests revealed highly significant ratio changes between ventralflexion to neutral curvature or dorsiflexion during sitting, $t(452) = 4.665$, $p < .001$ and $t(437) = 5.013$, $p < .001$, respectively, and standing, $t(436) = 5.216$, $p < .001$ and $t(467) = 6.245$, $p < .001$, respectively, while supine and lateral positions had no significant A_2/A_1 changes between curvatures. A_2/A_1 ratios in each position are shown in Figure 18B.

Finally, the interaction effect of curvature, muscle and position was not significant, $F(24,308) = 1,210$, $p = .231$.

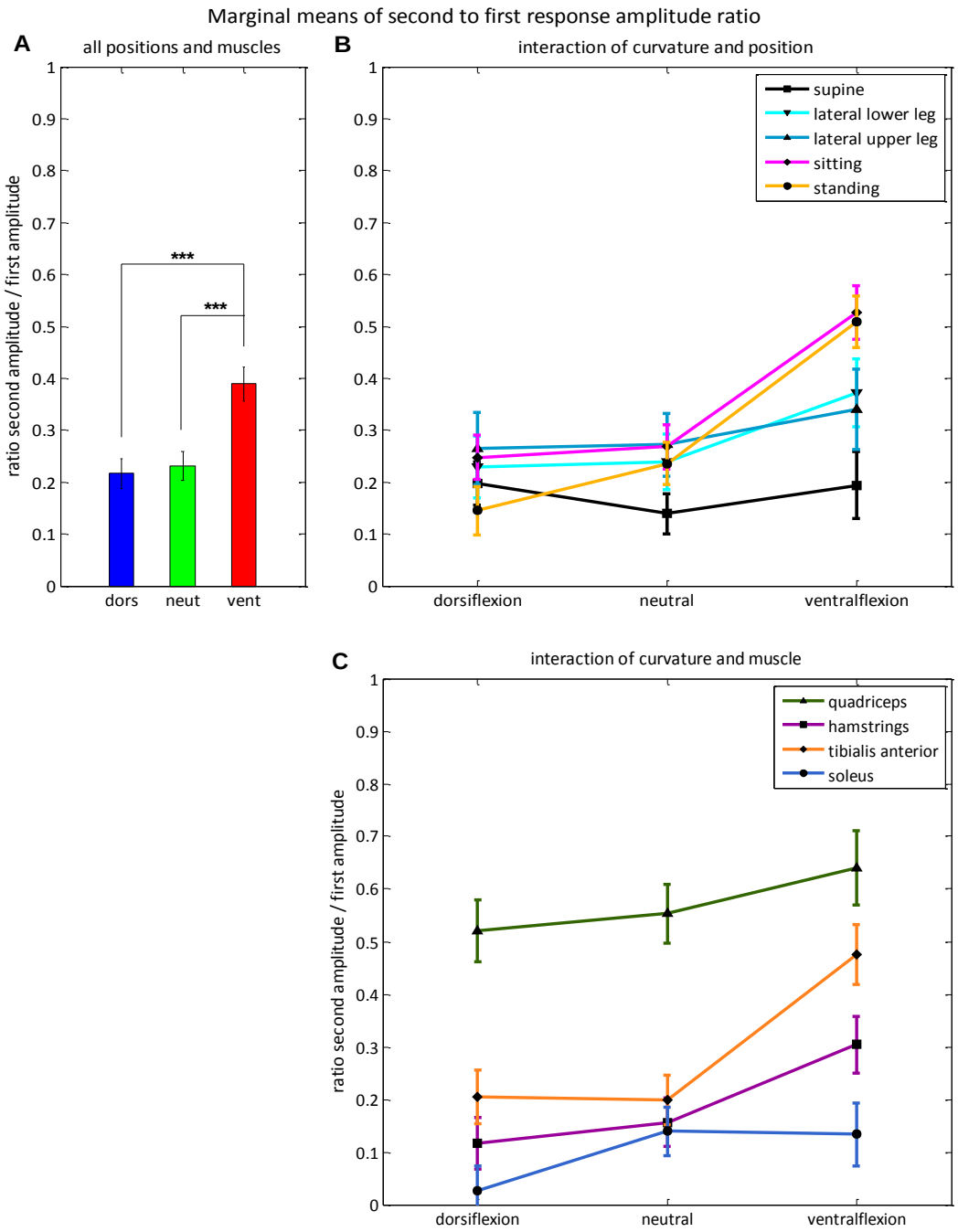

Figure 18 – Model estimates of marginal means and standard errors of A2/A1 ratios for each spinal curvature, across all positions and muscle groups (A), for each positions across all muscle groups (B) and for each muscle group across all positions (C). Brackets indicate significant differences (***: $p < .001$). Ventralflexion resulted in an overall significant ratio increase. In sitting and standing, this increase was present as well, while supine and lateral lying yielded no significant differences.

5. Discussion

Our findings show that lumbar ventralflexion of the spine during lumbar tSCS strongly decreased amplitudes of the first responses and increased the second to first response amplitude ratios compared to the neutral spine. Conversely, dorsiflexion had no significant effect on either of these parameters.

5.1. Relative excitation thresholds of stimulation hotspots

Effective PRM reflex elicitation can be characterized as the stimulation of afferent posterior root fibers with no or very little concomitant direct efferent anterior root activation. In contrasts to epidural stimulation, which produces a focused field close to the target structures, tSCS relies upon sites of lowered stimulation thresholds, to selectively target the posterior roots, while not inadvertently activating anterior roots. The activating function concept (Rattay, 1998; Rattay, 1999) predicts axon excitability as a function of the second spatial derivative of the extracellular potential along the axon, therefore at sites with tissue conductivity non-uniformities or bends along the axon trajectories within the electric field. Modeling studies (Rattay, et al., 2000; Ladenbauer, et al., 2010; Danner, et al., 2011; Danner, et al., 2014) have, for cathodic stimulation, identified these activation hotspots at the entry (posterior roots) into the spinal cord for the sensory, at the exit (anterior roots) from the spinal cord for the motor and at the common exit of the spinal nerves from the spinal canal for both sensory and motor fibers (Figure 19; Danner, et al., 2014). Therefore, posterior root activation necessitates sufficient transversal current through the spinal canal, and the relative excitation threshold depends on the current density at the stimulation hotspot. This current mainly enters through the intervertebral disks and ligaments (Ladenbauer, 2008), since their conductivity is thirty times higher than that of the spinous processes (Szava, 2006).

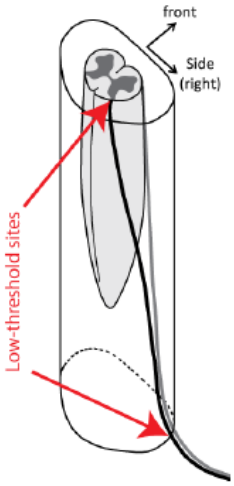

Figure 19 – Sketch of excitation hotspots found for cathodic tSCS (Danner, et al., 2014).

To differentiate between posterior (sensory) and anterior root (motor) stimulation, a paired stimulus paradigm can be used to investigate the nature of muscular responses to SCS (Courtine, et al., 2007; Minassian, et al., 2007b; Hofstoetter, et al., 2008; Dy, et al., 2010; Andrews, et al., 2015). Reflexes elicited at the sensory fibers are diminished when repeatedly activated because of post-activation depression and various other pre- and postsynaptic effects on the motoneurons (Minassian, et al., 2009), while responses to direct motor stimulation retain their amplitude. The extent of this depression depends on the ISI between the pulses, as well as their intensity (Minassian, et al., 2004), so the presence of a response to a pulse after previous stimulation does not necessarily indicate direct anterior root activation or a changed threshold ratio of the posterior root and anterior root hotspots. While stimulation intensities and ISI were kept constant across all spinal curvatures during one position in this study, an increased A_2/A_1 ratio from one curvature to another could either mean a decreased relative excitation threshold ratio of anterior to posterior roots, or a decreased posterior root threshold, thus increased relative sensory excitability, resulting in weaker suppression of A_2 without any additional anterior root excitation.

Therefore, a decreased anterior root threshold can only be conclusively assumed if an increased A_2/A_1 ratio is accompanied by a decreased or steady A_1. A_1 changes, on the other hand, indicate overall changes of activation thresholds, regardless of which hotspots are contributing to the muscle response.

During ventralflexion, first responses were decreased and second to first response ratio increased, indicating an increase in overall excitation thresholds and a decrease of the anterior to posterior threshold ratio. We propose that this is predominantly caused by an unfavorable current distribution within and around the spinal canal. Comparison of ventral- and dorsiflexion results suggest that the reason of this redistribution is two-fold: First, overall current density within the spinal canal decreases because of a higher transversal resistance of the spine from the smaller conductive intervertebral spaces of the inner side of the curvature, and secondly, a higher current density in the inner intervertebral spaces and lower density in the outer ones. The second cause alone would account for the lowered first response amplitudes and the decrease of the anterior to posterior threshold ratio for ventralflexion, but should result in the opposite effect for dorsiflexion – higher posterior current density and lower anterior density. Instead, dorsiflexion appeared to have no effect on stimulation efficacy. Lowered overall current density helps explain why dorsiflexion did not increase posterior relative excitation thresholds. It should be noted, though, that maximal achievable dorsiflexion was less than maximum ventralflexion, which could contribute to the lack of effects of dorsiflexion.

5.2. H reflex controlled main soleus: exclusion of reflex gain influences

Similar to the PRM reflex at low stimulation frequencies (Minassian, et al., 2012a), the H reflex is elicited in afferents with large diameters and predominantly activates α-motoneurons monosynaptically, except that the stimulation site is peripheral (Pierrot-Deseilligny & Burke, 2012). Therefore, to eliminate influences of posturally

changed reflex gain during tSCS on the response amplitudes, we elicited an H reflex in one soleus of each subject, at the popliteal fossa, where muscle responses were independent of geometry changes of the spinal cord and its surroundings. The M wave amplitude was kept constant to ensure stable stimulation conditions (Knikou, 2008), and the H reflex amplitude was monitored to ensure no reflex gain changes between curvatures. Therefore, our findings in the H reflex controlled soleus can be assumed to reflect changes of relative excitation thresholds caused by spinal geometry changes, rather than central reflex pathway modifications. They are similar to our overall results of all muscles: ventralflexion increased overall excitation thresholds and decrease the anterior to posterior ratio of relative excitation thresholds, indicating a change of current density distribution.

Another likely influence on relative excitation thresholds, as predicted by the activating function, are altered spinal nerve trajectories relative to the electric field (Danner et al., submitted). Different positions were measured to exclude position specific central or biophysical confounding effects from spinal curvature changes. Still, migration of the spinal cord within the spinal canal (Holsheimer, et al., 1994; Ranger, et al., 2008) as well as altered neural trajectories could also contribute to the diminished tSCS efficacy during ventralflexion in the soleus. Our results show decreased overall response amplitudes in ventralflexion in comparison to neutral curvature in all positions, while an increase of second to first response ratio could not be found in the supine position, where ratios were generally low. Lateral and sitting positions showed barely significant differences between ventralflexion and the other two curvatures, while standing showed the most pronounced increase during ventralflexion. It is unclear, though, whether these differences between positions stem from the influence of spinal nerve trajectories, the extent of achievable spinal curvature or other factors.

5.3. All muscle groups

Unlike the H reflex controlled main soleus, the relationship between the results obtained from the other seven recorded muscle groups and alteration of relative excitation thresholds is less decisive. Central reflex pathway gain is determined by a neural network of interconnected Ia, Ib and II afferent fibers of synergists and antagonists as well as corticospinal and vestibular inputs (Pierrot-Deseilligny & Burke, 2012). Therefore, even if the sum of all partial reflex gains of the main soleus equaled zero, posture induced reflex pathway gains in other muscles cannot be excluded. Overall though, we found A_1 and A_2/A_1 behavior upon spinal curvature to be similar to the H reflex controlled soleus, suggesting lessened tSCS efficacy during ventralflexion in all muscle groups, although the extent varied between muscles.

Figure 17C shows the order of A_1 changes with spinal curvature, the biggest differences seen in soleus, then hamstrings, tibialis anterior, and finally no changes in quadriceps, with the latter two below significance level. The caudocranial arrangement of spinal nerves innervating these muscle groups resembles that order: the soleus is supplied by S1-S2, hamstrings by L5-S2, tibialis anterior by L4-L5 and the quadriceps by L2-L4 spinal nerves (Palastanga & Soames, 2012), named after their exit sites through the intervertebral foramina. This arrangement is reflected by the A_2/A_1 magnitudes of the muscle groups as well (Figure 18C): spinal nerves whose anterior root hotspots are closest to the stimulating cathode located at T11-T12 show the highest ratios. Since an increase of A_2/A_1 with a simultaneous decrease of A_1, as observed in tibialis anterior and hamstrings from neutral curvature to ventralflexion, is indicative of a decrease in anterior to posterior root hotspot threshold ratio, the portion of A_1 that can change by an altered posterior root excitation threshold is diminished in these cases. This could account for the lower, but still significant A_1 changes we found in the hamstrings, where simultaneous A_2/A_1 changes were higher than in the soleus, and in the tibialis anterior, where A_1 changes were not significant

and A_2/A_1 changes were the greatest of all muscle groups. Additionally, assuming the overall A_2/A_1, regardless of spinal curvature, does indeed allow inferences about direct anterior root excitation, this further contributes to the A_1 change discrepancies, again decreasing the range of A_1 that is influenced by posterior root excitability. The quadriceps, the muscle group most likely to exhibit M wave contamination during lumbar tSCS (Minassian, et al., 2007b), showed the highest A_2/A_1 and exhibited almost no excitation threshold changes upon ventralflexion. It should be noted that a slight, if necessary, selection bias was introduced by limiting the inclusion of measurements for the A_2/A_1 analysis to cases with first response amplitudes above 0.1 mV, to exclude amplitudes that were small enough to be subject to large relative changes from confounding factors rather than representative muscle response changes, which excluded more quadriceps measurements than other muscle groups, limiting the A_2/A_1 change detection sensitivity in the quadriceps. Both solei, on the other hand showed high A_1 increase and no significant A_2/A_1 changes, which again supports this relation between A_1 and A_2/A_1 changes.

Since the craniocaudal order of spinal nerves is the same at their posterior root entry sites into the spinal cord, another possible contributing factor to the observed muscle group discrepancies could be spinal curvature consistently changing the geometry to a greater extent between more caudal vertebrae. A shift of the cathode relative to the spinal cord, on the other hand, seems unlikely: while a cranial shift from neutral curvature to ventralflexion would account for the absence of A_1 changes in more cranially innervated muscle groups, the observed anterior root excitation is not consistent with that.

The breakdown of positions (Figure 17B and Figure 18B) shows some differences between individual positions, most notably lowered first response amplitudes in the upper leg in the lateral position, compared to all other positions. We expect this stems from the gravitational migration of the spinal cord within the spinal canal

during lateral positions (Ranger, et al., 2008) and the resulting neural trajectories. Excluding the upper leg in the lateral position, we found similar effects of spinal curvature as in the H reflex controlled soleus: significantly lowered A_1 in all positions during ventralflexion, while A_2/A_1 showed the largest increase during standing and sitting and no differences during lateral and supine positions, with the latter again having the lowest ratios across all curvatures. Because of these similarities to the main soleus findings, we suggest that other factors beside altered reflex gain from lower limb joint angles or vestibular inputs contribute to these position discrepancies, like changed spinal cord location and neuron trajectories. To our knowledge, no imaging studies have compared the location of the spinal cord during supine, sitting and standing positions, which could help explain the position differences for anterior root excitation during ventralflexion.

6. Conclusion

Ventralflexion of the lumbar spine strongly lowers lumbar tSCS efficacy, both by decreasing overall reflex amplitudes and increasingly evoking direct motor responses. Therefore, we recommend tSCS application with a neutral (or dorsiflexed) spine. Our findings suggest altered transversal current distribution as the predominant cause, although changes of spinal cord location and spinal nerve trajectories may contribute as well. Modeling studies with different spinal curvatures could provide more insight into the current distribution and the underlying mechanisms of tSCS, and further electrophysiological studies measuring the extent of critical spinal flexion, not just maximum achievable curvatures like in this study, would be useful for practical applications.

Bibliography

Andrews, J., Stein, R. & Roy, F., 2015. Post-activation depression in the human soleus muscle using peripheral nerve and transcutaneous spinal stimulation. *Neuroscience Letters,* Volume 589, pp. 144-149.

Angeli, C., Edgerton, V., Gerasimenko, Y. & Harkema, S., 2014. Altering spinal cord excitability enables voluntary movements after chronic complete paralysis in humans. *Brain,* Volume 137, pp. 1394-1409.

Beam-Wiki, 2014. *beam-wiki.org.* [Online]
Available at: http://www.beam-wiki.org/wiki/Image:Typical_Neuron.GIF
[Accessed 10. 11. 2014].

Cook, A., 1976. Electrical stimulation in multiple sclerosis. *Hospital Practice,* Volume 11, pp. 51-58.

Cook, A. & Weinstein, S., 1973. Chronic dorsal column stimulation in multiple sclerosis, Preliminary report. *New York State Journal of Medicine,* Volume 73, pp. 2868-2872.

Courtine, G. et al., 2007. Modulation of multisegmental monosynaptic responses in a variety of leg muscles during walking and running in humans. *The Journal of Physiology,* Volume 582(3), pp. 1125-1139.

Danner, S. et al., 2015. Human spinal locomotor control is based on flexibly organized burst generators. *Brain,* Volume 138(3), pp. 577-588.

Danner, S. et al., 2014. Potential distribution and nerve fiber responses in transcutaneous lumbosacral spinal cord stimulation. In: S. Vlad & R. Ciupa, eds. *International conference on advancements of medicine and health care through technology; IFBME 44.* Switzerland: Springer International Publishing, pp. 203-208.

Danner, S. et al., 2011. Can the human lumbar posterior columns be stimulated by transcutaneous spinal cord stimulation? A modeling study. *Artificial Organs,* Volume 35, pp. 257-363.

Danner, S. et al., submitted. Body position influences which neural structures are recruited by lumbar transcutaneous spinal cord stimulation. *PLOS ONE.*

Dimitrijevic, M., 2012. Residual motor function after spinal cord injury. In: M. Dimitrijevic, B. Kakulas, W. McKay & G. Vrbova, eds. *Restorative neurology of spinal cord injury.* New York: Oxford University Press, Inc, pp. 1-9.

Dimitrijevic, M., Gerasimenko, Y. & Pinter, M., 1998. Evidence for a spinal central pattern generator in humans. *Annals of the New York Academy of Science,* Volume 860, pp. 360-376.

Dimitrijevic, M. et al., 1986. Spinal cord stimulation for the control of spasticity in patients with chronic spinal cord injury: II. Neurophysiologic observations. *Central Nervous System Trauma,* Volume 3, pp. 145-152.

Dy, C. et al., 2010. Phase-dependent modulation of percutaneously elicited multisegmental muscle responses after spinal cord injury. *Journal of Neurophysiology,* Volume 103, pp. 2808-2820.

Grace-Martin, K., 2015. *The analysis factor.* [Online]
Available at: http://www.theanalysisfactor.com/wacky-hessian-matrix/
[Accessed 25. 08. 2015].

Gu, W., Justiz, M. & Yao, H., 2002. Electrical conductivity of lumbar anulus fibrosis: effects of porosity and fixed charge density. *Spine,* Volume 27(21), pp. 2390-2395.

Harkema, S. et al., 2011. Effect of epidural stimulation of the lumbosacral spinal cord on voluntary mmovement, standing, and assisted stepping after motor complete paraplegia: a case study. *Lancet,* Volume 377, pp. 1938-1947.

Hayashi, R., Tako, K., Tokuda, T. & Yanagisawa, N., 1992. Comparison of amplitude of human soleus H-reflex during sitting and standing. *Neuroscience Research,* Volume 13, pp. 227-233.

Herman, R. et al., 2002. Spinal cord stimulation facilitates functional walking in a chronic, incomplete spinal cord injured. *Spinal cord,* Volume 40, pp. 65-68.

Hofstoetter, U. et al., 2014b. Neuromodulation of voluntary locomotor activity by transcutaneous spinal cord stimulation in motor-incomplete spinal cord injured individuals: A preliminary study. *Artificial Organs,* Volume 37(2), pp. 202-211.

Hofstoetter, U. et al., 2014a. Modification of spasticity by transcutaneous spinal cord stimulation in individuals with incomplete spinal cord injury. *Journal of Spinal Cord Medicine,* Volume 37, pp. 202-211.

Hofstoetter, U. et al., 2008. Modification of reflex responses to lumbar posterior root stimulation by motor tasks in healthy subjects. *Artificial Organs,* Volume 32, pp. 644-648.

Holsheimer, J., 1998a. Concepts and methods in neuromodulation and functional electrical stimulation: an introduction. *Neuromodulation,* Volume 1(2), pp. 57-61.

Holsheimer, J., 1998b. Computer modeling of spinal cord stimulation and its contribution to therapeutic efficacy. *Spinal Cord,* Volume 36, pp. 531-540.

Holsheimer, J., den Boer, J., Struijk, J. & Rozeboom, A., 1994. MR assessment of the normal position of the spinal cord in the spinal canal. *American Journal of Neuroradiology,* Volume 15, pp. 951-959.

Iles, J. & Pisini, J., 1992. Vestibular-evoked postural reactions in man and modulation of transmission in spinal reflex pathways. *Journal of Physiology,* Volume 455, pp. 407-424.

Jilge, B., Minassian, K. & Rattay, F. e. a., 2004. Initiating extension of lower limbs in subjects with complete spinal cord injury by epidural lumbar cord stimulation. *Experimental Brain Research,* Volume 154, pp. 308-326.

Kandel, E. et al., 2013. *Principles of neural science.* 5th ed. s.l.:McGraw-Hill Companies, Inc.

Kitano, K. & Koceja, D., 2009. Spinal reflex in human lower leg muscles evoked by transcutaneous spinal cord stimulation. *Journal of Neuroscience Methods,* Volume 180, pp. 111-115.

Knikou, M., 2008. The H-reflex as a probe: Pathways and pitfalls. *Journal of Neuroscience Methods,* Volume 171, pp. 1-12.

Knikou, M., 2013. Neurophysiological characterization of transpinal evoked potentials in human leg muscles. *Bioelectromagnetics,* Volume 34, pp. 630-640.

Kudina, L., Ashby, P. & Downes, L., 1993. Effects of cortical stimulation on reciprocal inhibition in humans. *Experimental Brain Research,* Volume 94, pp. 533-538.

Ladenbauer, J., 2008. Simulation of the excitation of human lower spinal cord structures with surface electrodes: 3D finite element analysis and nerve fiber modeling. *MA Thesis, Vienna University of Technology.*

Ladenbauer, J. et al., 2010. Stimulation of the human lumbar spinal cord with implanted and surface electrodes: a computer simulation study. *IEEE Transactions on Neural Systems and Rehabilitation Engineering,* Volume 18, pp. 637-645.

Meunier, S. & Pierrot-Deseilligny, E., 1998. Cortical control of presynaptic inhibition of Ia afferents in humans. *Experimental Brain Research,* Volume 119, pp. 415-426.

Minassian, K. et al., 2015. Spinal rhythm generation by step-induced feedback and transcutaneous posterior root stimulation in complete spinal cord-injured individuals. *Neurorehabilitation & Neural Repair, doi: 10.1177/1545968315591706.*

Minassian, K., Hofstoetter, U. & Rattay, F., 2012a. Transcutaneous lumbar posterior root stimulation for motor control studies and modification of motor activity after spinal cord injury. In: M. Dimitrijevic, B. Kakulas, W. McKay & G. Vrbova, eds. *Restorative Neurology of Spinal Cord Injury.* New York: Oxford University Press, Inc, pp. 226-255.

Minassian, K. et al., 2009. *Posterior root-muscle reflexes and the H reflex in humans: Electrophysiological comparison.* In Program No. 658.12.2009 Neuroscience Meeting Planner, Chicago: Society for Neuroscience, 2009.

Minassian, K., Hofstoetter, U., Tansey, K. & Mayr, W., 2012b. Neuromodulation of lower limb motor control in restorative neurology. *Clinical Neurology and Neurosurgery,* Volume 114, pp. 489-497.

Minassian, K. et al., 2004. Stepping-like movements in humans with complete spinal cord injury induced by epidural stimulation of the lumbar cord: electromyographic study of compound muscle action potentials. *Spinal Cord,* Volume 42, pp. 401-416.

Minassian, K., Persy, I., Rattay, F. & Dimitrijevic, M., 2005. Effect of peripheral afferent and central afferent input to the human lumbar spinal cord isolated from brain control. *Biocybernetics and Biomedical Engineering,* Volume 25, pp. 11-29.

Minassian, K. et al., 2007b. Posterior root-muscle reflexes elicited by transcutaneous stimulation of the human lumbosacral cord. *Muscle and Nerve,* Volume 35, pp. 327-336.

Minassian, K. et al., 2007a. Human lumbar cord circuitries can be activated by extrinsic tonic input to generate locomotor-like activity. *Human Movement Science,* Volume 26, pp. 275-295.

Murg, M., Binder, H. & Dimitrijevic, M., 2000. Epidural electric stimulation of posterior structures of the human lumbar spinal cord: 1. Muscle twitches - a multifunctional method to define the site of stimulation. *Spinal cord,* Volume 38, pp. 394-402.

My-MS, 2014. *My-MS.org.* [Online]
Available at: http://www.my-ms.org/anatomy_nervous_system.htm
[Accessed 10. 11. 2014].

Nielsen, J., Petersen, N., Deuschl, G. & Ballegaard, M., 1993. Task-related changes in the effect of magnetic brain stimulation on spinal neurones in man. *Journal of Physiology,* Volume 471, pp. 223-243.

Nowak, L. & Bullier, J., 1998. Axons, but not cell bodies, are activated by electrical stimulation in cortical gray matter. II. Evidence from selective inactivation of cell bodies and axon initial segments.. *Experimental Brain Research,* Volume 118, pp. 489-500.

O'Rahilly, R., Müller, F., Carpenter, S. & Swenson, R., 2004. *Basic human anatomy.* [Online]
Available at: https://www.dartmouth.edu/~humananatomy/part_7/chapter_41.html
[Accessed 10. 11. 2014].

Palastanga, N. & Soames, R., 2012. *Anatomy and human movement.* s.l.:Elsevier, Lt..

Pierrot-Deseilligny, E. & Burke, D., 2012. *The circuitry of the human spinal cord: spinal and corticospinal mechanisms of movement.* 1st ed. New York: Cambridge University Press.

Pinter, M., Gerstenbrand, F. & Dimitrijevic, M., 2000. Epidural electrical stimulation of posterior structures of the human lumbosacral cord: 3. Control of spasticity. *Spinal Cord,* Volume 38, pp. 524-531.

Porter, R., 1963. Focal stimulation of hypoglossal neurons in the cat. *Journal of Physiology,* Volume 169, pp. 630-640.

Purves, D. et al., 2004. *Neuroscience.* 3rd ed. Sunderland, MA, USA: Sinauer Associates, Inc.

Ranck, J., 1975. Which elements are excited in electrical stimulation of mammalian central nervous system: A review. *Brain Research,* Volume 98, pp. 417-440.

Ranger, M., Irwin, G., Bunbury, K. & Peutrell, J., 2008. Changing body position alters the location of the spinal cord within the vertebral canal: a magnetic resonance imaging study. *British Journal of Anaesthesia,* Volume 101(6), pp. 804-809.

Rattay, F., 1987. Ways to approximate current-distance relations for electrically stimulated fibers. *Journal of Theoretical Biology,* Volume 125, pp. 339-349.

Rattay, F., 1990. *Electrical Nerve Stimulation.* Vienna: Springer.

Rattay, F., 1998. Analysis of the electric excitation of CNS neurons. *IEEE Transactions on Biomedical Engineering,* Volume 45, pp. 766-772.

Rattay, F., 1999. The basic mechanism for the electrical stimulation of the nervous system. *Neuroscience,* Volume 89, pp. 335-346.

Rattay, F., Minassian, K. & Dimitrijevic, M., 2000. Epidural electrical stimulation of posterior structures of the human lumbosacral cord: 2. Quantitative analysis by computer modeling. *Spinal Cord,* Volume 38, pp. 473-489.

Rosenfeld, J., Sherwood, A., Halter, J. & Dimitrijevic, M., 1995. Evidence of a pattern generator in paralyzed subject with spinal cord stimulation. *Society for Neuroscience Abstracts,* Volume 21, p. 688.

Rossi, A., Mazzocchio, R. & Scarpini, C., 1988. Changes in Ia reciprocal inhibition from the peroneal nerve to soleus alpha-motoneurons with different static body position in man. *Neuroscience Letters,* Volume 84, pp. 283-286.

Roth, B., 1994. Mechanisms for electrical stimulation of excitable tissue. *Critical Reviews in Biomedical Engineering,* Volume 22, pp. 253-305.

Roy, F., Gibson, G. & Stein, R., 2012. Effect of percutaneous stimulation at different spinal levels on the activation of sensory and motor roots. *Experimental Brain Research,* Volume 223, pp. 281-289.

Schwan, H. & Kay, C., 1957. Capacitive properties of body tissues. *Circulation Research,* Volume 5(4), pp. 439-443.

Shapkova, E., 2004. Spinal locomotor capability revealed by electrical stimulation of the lumbar enlargment in paraplegic patients. In: M. Latash & M. Levin, eds. *Progress in motor control, vol.3: Effect of Age, Disorder, and Rehabilitation.* Champaign, IL: Human Kinetics, pp. 253-289.

Struijk, J. et al., 1993. Paresthesia thresholds in spinal cord stimulation: A comparison of theoretical results with clinical data. *IEEE Transactions on Rehabilitation Engineering,* Volume 1(2), pp. 202-108.

Struijk, J., Holsheimer, J., van der Heide, G. & Boom, H., 1992. Recruitment of dorsal column fibers in spinal cord stimulation: influence of collateral branching. *IEEE Transactions on Biomedical Engineering,* Volume 39(9), pp. 903-912.

Struijk, J., Holsheimer, J., van Veen, B. & Boom, H., 1991. Epidural spinal cord stimulation: calculation of field potentials with special reference to dorsal column nerve fibers. *IEEE Transactions on Biomedical Engineering,* Volume 38(1), pp. 104-110.

Szava, Z., 2006. Three-dimensional finite element simulation of the electrical field distribution within the vertebral canal generated by surface electrodes. *MA Thesis, University of Applied Sciences Technikum Wien.*

Wikipedia, 2014. *Wikipedia, the free encyclopedia.* [Online]
Available at: https://en.wikipedia.org/w/index.php?title=Spinal_cord&oldid=339359433
[Accessed 10. 11. 2014].

Wikipedia, 2015. *Wikipedia, the free encyclopedia.* [Online]
Available at: https://en.wikipedia.org/wiki/Supraspinous_ligament
[Accessed 15. 07. 2015].